Inclusive hadroproduction of charmonia-bottomonia pairs in the CGC framework

Marat Siddikov

Departamento de Física, Universidad Técnica Federico Santa María, y Centro Científico–Tecnológico de Valparaíso, Casilla 110-V, Valparaíso, Chile

(Received 29 March 2025; accepted 29 July 2025; published 8 September 2025)

In this paper, we analyze the inclusive hadroproduction of heavy charmonia-bottomonia pairs in the color glass condensate framework in the dilute-dense approximation. The production mechanisms can be classified by the number of gluons emitted from projectiles as single- and double-parton scattering. We analyzed separately both types of contributions and evaluated the corresponding impact factors in the leading order in strong coupling α_s. For the double-parton scattering, the impact factors factorize into a product of impact factors of single charmonia and bottomonia production cross sections, and the cross section in the large-N_c limit reduces to the well-known pocket formula. For the single-parton scattering, we found that the cross section of the process is sensitive to dipole, quadrupole, sextupole, and octupole scattering amplitudes (correlators of Wilson lines), thus opening possibility to study phenomenologically these novel objects. We also made phenomenological estimates of the cross sections in the dilute approximation and found that the provided approach provides a fair qualitative description of the LHCb data for $J/\psi + \Upsilon(1S)$ production.

DOI: 10.1103/cz6q-3w6d

I. INTRODUCTION

The quarkonia have been considered as useful probes of the gluonic field of the target almost since their discovery. The small sizes of the quarkonia and the heavy masses of the constituent quarks, which play the role of the natural hard scales, motivated application of various perturbative schemes for description of their production. The hadronization of heavy quarks into quarkonia at present is understood reasonably well and is described in the nonrelativistic QCD (NRQCD) framework, which encodes it in terms of the nonperturbative long distance matrix elements (LDMEs) of quarkonia states [1–5]. This approach allows us to get reasonable estimates for the cross sections, and for this reason (single) quarkonia production is being included in phenomenological fits of the gluonic generalized parton distributions and color dipole cross sections [6–8] which control the cross section in this channel in different kinematics. From this point of view, the production of multiple quarkonia, especially the heavy quarkonia pairs, presents an interesting tool which can be used to improve our understanding of the heavy quarkonia formation. Such channels attracted theoretical attention since the early days of QCD [9–12], and the possibility to study such channels experimentally was demonstrated soon afterwards [13,14]. Recent experiments at the LHC demonstrated a possibility to study the production of quarkonia pairs with reasonably high precision.

In this paper, we focus on the associated production of charmonia and bottomonia pairs, which has a very simple structure of the partonic amplitude. The theoretical studies of such processes (particularly, $J/\psi + \Upsilon$ hadroproduction) have been initiated in Refs. [15–17] and attracted a lot of theoretical attention. In the collinear and k_T factorization approach, it is known that the contribution of single-parton scattering in such processes is strongly suppressed by a strong coupling α_s^2 compared to production of quarkonia pairs with the same hidden flavor. For this reason, the suggested processes have been suggested as a possible tool for studies of various mechanisms that are usually suppressed and controlled by the poorly known color octet long distance matrix elements or the double-parton distribution functions (DPDFs). The recent experimental data [18,19] demonstrated that the contribution controlled by DPDFs indeed may be significant in this channel. However, at present the situation remains unclear: while inclusion of the DPDFs allows us to explain the difference between the data and predictions based on single-parton scattering, the value of the so-called parameter σ_{eff}, which controls the magnitude of the DPDFs, depends significantly on the channel used for its extraction [20–22]. This discrepancy hints that this channel in the small-x kinematics potentially

Published by the American Physical Society under the terms of the Creative Commons Attribution 4.0 International license. Further distribution of this work must maintain attribution to the author(s) and the published article's title, journal citation, and DOI. Funded by SCOAP³.

can get contributions from other mechanisms, which eventually lead to onset of saturation effects, and for this reason it is appropriate to analyze this process in the frameworks with built-in saturation. In what follows, we will realize such study using the color glass condensate (CGC) framework [23–27], which naturally incorporates the saturation effects and provides a phenomenologically reasonable description of both hadron-hadron and lepton-hadron collisions [7,28–41]. The cross sections of physical processes in this framework are expressed in terms of the forward multipole scattering amplitudes (n-point correlators of Wilson lines), which present important physical characteristics of the target. In some special cases, these correlators may be related to the forward dipole scattering amplitudes, which are well known from the phenomenology.

The paper is structured as follows: in Sec. II, we briefly describe the main components of the CGC framework and then present the theoretical results for the hadroproduction of heavy quarkonia pairs in the CGC approach. In Sec. III, we provide rough numerical estimates for the cross sections using very simple parametrization for quadrupoles, sextupoles, and octupoles inspired by dilute limit. We demonstrate that the suggested approach is in fair qualitative agreement with experimental data. More accurate estimates using elaborate parametrizations of quadrupole, sextupole, and octupole amplitudes entail significant computational challenges and will be presented elsewhere. Finally, in Sec. IV, we draw conclusions.

II. THEORETICAL FRAMEWORK

In what follows, we will analyze the hadroproduction of the quarkonia pairs in a dilute-dense limit. This treatment is justified in the forward kinematics, when the produced quarkonia propagate in direction of one of the colliding hadrons (the "projectile"). If the rapidity difference between any given quarkonium and the projectile does not exceed a few units, the interaction of the latter with heavy quarks forming the quarkonia can be described in the partonic picture, disregarding possible saturation effects. At the same time, as the partons move with very high energies with respect to another hadron (the "target"), the CGC framework should be applied in order to describe this interaction and onset of the saturation effects.

The production of the heavy quarkonia pair in this picture may be considered as a result of the scattering of one or two gluons emitted from the projectile in the field of the target. In what follows we will refer to these processes as single- and double-parton scattering (SPS and DPS, respectively, see Fig. 1 for illustration), in agreement with the terminology used in the analyses based on the collinear and k_T-factorization (see Ref. [22] for a review). In Sec. II A, we introduce our notations and the light-cone decomposition of the particle's momenta. In Sec. II B, we briefly introduce the color glass condensate approach [23–26,42–47], which will be used for theoretical evaluations. Finally, in Secs. II C and II D, we derive the expressions for the contributions of SPS and DPS mechanisms.

A. Kinematics of the process

In what follows, we will work in the gluon-proton scattering frame and assume that the momentum of the target and the total momentum of the gluons(s) emitted from the projectile point in the direction of axis z. We will use a notation q for the momentum of the incoming gluon in the SPS mechanism, $\mathbf{q}_1$, $\mathbf{q}_2$ for the momenta of incoming (projectile) gluons in DPS mechanism, P for the target momentum, and p_1, p_2 for the momenta of the produced quarkonia. For the sake of definiteness, we will use the Kogut-Soper convention [48] for the light-cone components of all the vectors, and boldface letters with subindex $\perp$ for the transverse (1,2)-components, namely

$$v^\mu = (v^+, v^-, \boldsymbol{v}_\perp), \qquad v^\pm = \frac{v^0 \pm v^3}{\sqrt{2}},$$
$$\boldsymbol{v}_\perp = v_x \hat{\boldsymbol{x}} + v_y \hat{\boldsymbol{y}}. \tag{1}$$

The square of the vector in this convention is given by

$$v^2 \equiv v^\mu v_\mu = 2v^+v^- - \boldsymbol{v}_\perp^2, \tag{2}$$

and the convolution with Dirac γ-matrix reads as

$$\hat{v} = \gamma^\mu v_\mu = \gamma^+ v^- + \gamma^- v^+ - \boldsymbol{\gamma}_\perp \cdot \boldsymbol{v}_\perp. \tag{3}$$

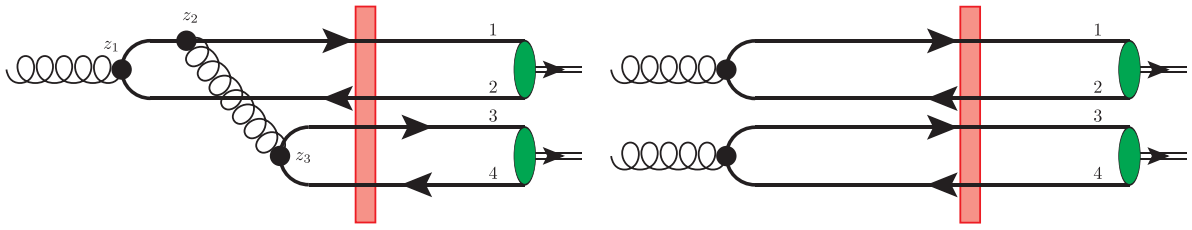


FIG. 1. Example diagrams describing the inclusive heavy quarkonia pair production in SPS and DPS. The red block represents a shock wave in the CGC picture.

The light-cone decomposition of the momentum P of the target (proton) and the momenta p_1, p_2 of the produced quarkonia are given by

$$P = \left(\frac{m_N^2}{2P^-}, P^-, \mathbf{0}_\perp\right),$$
$$P^- = \frac{E_p + \sqrt{E_p^2 - m_N^2}}{\sqrt{2}} \approx \sqrt{2}E_p \tag{4}$$

$$p_a = \left(M_{a,\perp}e^{y_a}, \frac{M_{a,\perp}e^{-y_a}}{2}, \boldsymbol{p}_a^\perp\right),$$
$$M_{a,\perp} \equiv \sqrt{M_a^2 + (\boldsymbol{p}_a^\perp)^2}, \quad a = 1, 2, \tag{5}$$

where $(y_a, \boldsymbol{p}_a^\perp)$ are the rapidities and transverse momenta of the produced quarkonia with respect to the collision axis, M_a are their masses, and m_N is the mass of the nucleon. In this paper, we will be mostly interested in the high-energy collider kinematics, when quarkonia are produced with relatively small transverse momenta. In these kinematics, it is possible to use the eikonal picture and assume that the plus component q_a^+ of the incoming gluon light-cone momentum is shared only between the produced quarkonia. This allows us to write out the light-cone decomposition of the incoming photon momentum in the SPS process as

$$q = (q^+, 0, \mathbf{0}_\perp), \qquad q^+ = M_{1,\perp}e^{y_1} + M_{2,\perp}e^{y_2}. \tag{6}$$

Similarly, for a pair of two incoming gluons in the DPS kinematics, we may assume that the momenta of the gluons emitted from the projectile are given by

$$\mathfrak{q}_a = (M_{a,\perp}e^{y_a}, 0, \boldsymbol{\mathfrak{q}}_{a,\perp}), \quad a = 1, 2. \tag{7}$$

For the sake of brevity, sometimes we will use notations

$$\alpha_1 = \frac{M_{1,\perp}e^{y_1}}{M_{1,\perp}e^{y_1} + M_{2,\perp}e^{y_2}},$$
$$\alpha_2 = 1 - \alpha_1 = \frac{M_{2,\perp}e^{y_2}}{M_{1,\perp}e^{y_1} + M_{2,\perp}e^{y_2}},$$

which allow us to rewrite the momenta of the quarkonia in the compact form as

$$p_a = \left(\alpha_a q^+, \frac{M_{a,\perp}^2}{2\alpha_a q^+}, \boldsymbol{p}_a^\perp\right), \quad a = 1, 2,$$

$$q_{(\mathrm{SPS})} = (q^+, 0, \mathbf{0}_\perp), \qquad \mathfrak{q}_a = (\alpha_a q^+, 0, \boldsymbol{\mathfrak{q}}_{a,\perp}). \tag{8}$$

The invariant energy W of the gluon-proton collision and the invariant mass M_{12} of the produced heavy quarkonia pair may be expressed as

$$W^2 \equiv (q+P)^2 = -Q^2 + m_N^2 + 2q\cdot P$$
$$\approx -m_N^2 + 2P^-(M_1^\perp e^{y_1} + M_2^\perp e^{y_2}), \tag{9}$$

and

$$\mathcal{M}_{12}^2 = (p_1+p_2)^2 = M_1^2 + M_2^2$$
$$+ 2(M_1^\perp M_2^\perp \cosh\Delta y - \boldsymbol{p}_1^\perp\cdot\boldsymbol{p}_2^\perp), \tag{10}$$

respectively. In order to avoid possible (soft) final state interactions between quarkonia, in what follows we will tacitly assume that these heavy mesons are kinematically well separated from each other, namely that the invariant mass $\mathcal{M}_{12}^2$ is sufficiently large, thus avoiding a near-threshold production.

B. High-energy scattering in the CGC picture

In the CGC framework, which is valid in the small-x (high-energy) kinematics, the interaction of the heavy parton with the target in configuration space is described in eikonal approximation, and is given by the Wilson line $U(\boldsymbol{x}_\perp)$ [23–27,43,44], as follows:

$$U(\boldsymbol{x}_\perp) = P\exp\left(ig\int dx^- A_a^+(x^-, \boldsymbol{x}_\perp)t^a\right), \tag{11}$$

where $\boldsymbol{x}_\perp$ is the transverse coordinate (impact parameter) of the parton, and t_a are the generators of the color group generators in the corresponding representation ($\mathbf{3}$, $\bar{\mathbf{3}}$, or 8 for quark, antiquark, and gluon, respectively), $A_\mu^a(x)$ is the semiclassical gluonic field created color charge distributed with density $\rho_a(\boldsymbol{x})$, with $A_\mu^a(x) = -\frac{1}{\nabla_\perp^2}\rho_a(x^-, \boldsymbol{x}_\perp)$. In the momentum space, the interactions of the partons with the target can be rewritten as CGC Feynman rules [34,49–51] provided in Table I. The prefactor $2\pi\delta(\ell^+ - \ell'^+)$ in all the shock wave interaction vertices reflects conservation of the plus component and sometimes is rewritten in the literature as

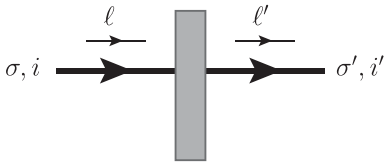
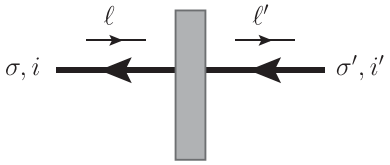
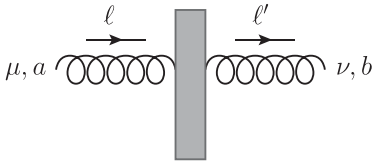
$$2\pi\delta(\ell^+ - \ell'^+) = \int_{-\infty}^{+\infty} dz^- e^{i(\ell^+ - \ell'^+)z^-}. \tag{12}$$

In general, the Wilson line (11) depends on color charge configurations $\rho(x^-, \boldsymbol{x}_\perp)$, whose probability in the CGC framework is described by the target-dependent weight functional $W[\rho]$ [23–25]. The physical observables can be obtained averaging over all possible configurations $\rho(x^-, \boldsymbol{x}_\perp)$, namely

$$\langle\mathcal{A}\rangle = \int \mathcal{D}\rho W[\rho]\mathcal{A}[\rho], \tag{13}$$

where $\mathcal{A}[\rho]$ corresponds to observable found for a fixed distribution of charges $\rho(x^-, \boldsymbol{x}_\perp)$, and the angular

TABLE I. CGC Feynman rules for the interaction of the partons with the shock wave (vertical gray block) [34,49–51]. We use the notations ℓ, ℓ' for the momenta of the partons before and after interaction with the shock wave, σ, σ' for Dirac indices of the quarks, i, i' for the color indices in the fundamental representations **3** or $\bar{\mathbf{3}}$, and a, b for the gluon color indices in the adjoint irreducible representation **8** of the color group. The matrices U and $\mathcal{U}$ are the Wilson lines in the fundamental and the adjoint representations, respectively.

	The interaction vertex of the quark with the shock wave: $T^{Q}_{\sigma,\sigma';i,i'} = 2\pi\delta(\ell^+ - \ell'^+)\gamma^+_{\sigma',\sigma}\int d^2z e^{i(\boldsymbol{\ell}-\boldsymbol{\ell}')\cdot z}[U(z)-1]_{i',i}$
	The interaction vertex of the antiquark with the shock wave: $T^{\bar{Q}}_{\sigma,\sigma';i,i'} = -2\pi\delta(\ell^+ - \ell'^+)\gamma^+_{\sigma,\sigma'}\int d^2z e^{i(\boldsymbol{\ell}-\boldsymbol{\ell}')\cdot z}[U^\dagger(z)-1]_{i,i'}$
	The interaction vertex of the gluon with the shock wave: $T^{g}_{\mu,\nu;a,b} = -2\pi\delta(\ell^+ - \ell'^+)g_{\mu\nu}\mathrm{sgn}(\ell^+) \times \int d^2z e^{-i(\boldsymbol{\ell}'-\boldsymbol{\ell})\cdot z}[\mathcal{U}^{\mathrm{sgn}(\ell^+)}(z)-1]_{b,a}$

brackets $\langle\ldots\rangle$ imply the above-mentioned averaging. The analytic evaluation of the integral $\mathcal{D}\rho$ is possible only for simple forms of $W[\rho]$, like, e.g., for the Gaussian parametrization implemented in Refs. [23,24]. Fortunately, many observables can be expressed via universal target-dependent correlators of several Wilson lines, which can be interpreted as multipole scattering amplitudes and can be extracted from phenomenological analysis. For example, in many processes which involve production of heavy quarks and antiquarks, the interaction with the target after averaging over the color charges (13) reduces to the nonperturbative dipole S-matrix element [26,27,52]

$$S_2(Y,\boldsymbol{x}_q,\boldsymbol{x}_{\bar{q}}) = \frac{1}{N_c}\langle \mathrm{tr}(U(\boldsymbol{x}_q)U^\dagger(\boldsymbol{x}_{\bar{q}}))\rangle_Y, \qquad (14)$$

where we use notation Y for the rapidity of the dipole. The phenomenological parametrizations of $S_2(Y,\boldsymbol{x}_q,\boldsymbol{x}_{\bar{q}})$ frequently are given in terms of the dipole scattering amplitude $N(x,\boldsymbol{r},\boldsymbol{b})$, which is related to $S_2(Y,\boldsymbol{x}_q,\boldsymbol{x}_{\bar{q}})$ as

$$N(x,\boldsymbol{r},\boldsymbol{b}) = 1 - S_2\left(Y = \ln\left(\frac{1}{x}\right), \boldsymbol{x}_q, \boldsymbol{x}_{\bar{q}}\right), \qquad (15)$$

where we introduced the variables $\boldsymbol{r} \equiv \boldsymbol{x}_q - \boldsymbol{x}_{\bar{q}}$ and $\boldsymbol{b} \equiv \alpha_q\boldsymbol{x}_q + \alpha_{\bar{q}}\boldsymbol{x}_{\bar{q}}$ for the transverse size and the transverse position of the dipole's center of mass. Similarly, the processes which involve multiple heavy quarks are sensitive to the multipole scattering S-matrix elements (correlators of Wilson lines)

$$S_{2n}(Y,\boldsymbol{x}_1,\boldsymbol{\xi}_1,\ldots,\boldsymbol{x}_n,\boldsymbol{\xi}_n) = \frac{1}{N_c}\langle \mathrm{tr}(U(\boldsymbol{x}_1)U^\dagger(\boldsymbol{\xi}_1)\ldots U(\boldsymbol{x}_n)U^\dagger(\boldsymbol{\xi}_n))\rangle_Y, \qquad (16)$$

which correspond to the scattering amplitudes of $2n$-particle ensemble of quarks. Such correlators represent important characteristics of the target related to the gluon distributions of the latter. The higher-order correlators reduce to the correlators of lower order in some special limits (for example, when the neighbor arguments coincide, $\boldsymbol{x}_i = \boldsymbol{\xi}_i$ or $\boldsymbol{x}_i = \boldsymbol{\xi}_{i-1}$). However, it is not possible to express higher-order correlators solely in terms of the correlators of lower-order in a model-independent way, as the former are more general objects.

Finally, we would like to mention that the structure of the shock wave vertices allows us to represent the corresponding perturbative impact factors, which appear in front of different correlators $S_{2n}(Y,\boldsymbol{x}_1,\boldsymbol{\xi}_1,\ldots,\boldsymbol{x}_n,\boldsymbol{\xi}_n)$ in physical observables, as a convolution of the light-cone wave functions of the partonic ensemble of the initial and final states. Indeed, let us consider for the sake of definiteness the diagram shown in Fig. 2 (this process is not directly related to heavy quarkonia pair production and is chosen merely for illustration due to its simplicity; its extension to arbitrary number of partons interacting with the shock wave is straightforward).

The matrices $U, U^\dagger$ are diagonal in helicity (Dirac) space, and for this reason may be disregarded (factorized and taken out) when analyzing Dirac algebra. The propagators of the free quarks and antiquarks are given by

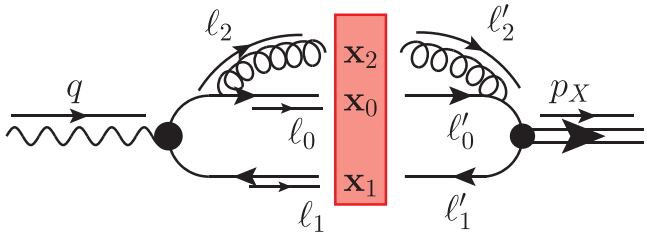


FIG. 2. Typical diagram showing interaction of the quark, antiquark, and gluon with the shock wave (we use notations with respective subindices 0,1,2 to distinguish their coordinates). The primed momenta $(\ell'_0, \ell'_1, \ell'_2)$ correspond to momenta after interaction with the shock wave (red block). The dummy variables $\boldsymbol{x}_0$, $\boldsymbol{x}_1$, $\boldsymbol{x}_2$ are the configuration-space transverse coordinates of the partons during interaction with the shock wave. See the text for a more detailed explanation.

$$S(k) = i\frac{\hat{k}+m}{k^2-m^2}, \tag{17}$$

and for on shell quarks ($k^2 = m^2$), we may rewrite numerator using conventional identities

$$\sum_h u_h(k)\bar{u}_h(k) = \hat{k}+m,$$
$$\sum_h v_h(\bar{k})\bar{v}_h(\bar{k}) = \hat{k}-m. \tag{18}$$

For the propagators of the off shell fermions which pass through the shock wave, we may rewrite the numerators as

$$\begin{aligned}\hat{k}\mp m &= \left(\gamma^+\frac{\boldsymbol{k}_\perp^2+m^2}{2k^+} + \gamma^- k^+ - \boldsymbol{\gamma}_\perp\cdot\boldsymbol{k}_\perp \mp m\right) \\ &\quad + \gamma^+\left(k^- - \frac{\boldsymbol{k}_\perp^2+m^2}{2k^+}\right) \\ &= \begin{cases}\sum_h u_h(\tilde{k})\bar{u}_h(\tilde{k}) \\ \sum_{\bar{h}} v_{\bar{h}}(\tilde{k})\bar{v}_{\bar{h}}(\tilde{k})\end{cases} + \gamma^+\left(k^- - \frac{\boldsymbol{k}_\perp^2+m^2}{2k^+}\right), \\ \tilde{k} &= \left(k^+, \frac{\boldsymbol{k}_\perp^2+m^2}{2k^+}, \boldsymbol{k}_\perp\right).\end{aligned} \tag{19}$$

Using the fact that the shock wave includes multiplication by γ^+ together with identity $\gamma^+\gamma^+ = 0$, we may see that the last term $\sim\gamma^+$ in the last line does not contribute. Finally, using the identities

$$\begin{aligned}\bar{u}_{h_1}(p_1)\gamma^+ u_{h_2}(p_2) &= \bar{v}_{h_1}(p_1)\gamma^+ v_{h_2}(p_2) \\ &= 2\sqrt{p_1^+ p_2^+}\,\delta_{h_1,h_2},\end{aligned} \tag{20}$$

we may obtain the set of identities

$$(\hat{\ell}'+m)T^Q_{i,i'}(\hat{\ell}+m) = 2\pi\int d^2\boldsymbol{x}[U(\boldsymbol{x})-1]_{i',i}\sum_h\left[u_h\left(\ell^+, \frac{(\boldsymbol{\ell}'_\perp)^2+m^2}{2\ell^+}, \boldsymbol{\ell}'_\perp\right)e^{-i\boldsymbol{\ell}'\cdot\boldsymbol{x}}\right]\left[\bar{u}_h\left(\ell^+, \frac{\boldsymbol{\ell}_\perp^2+m^2}{2\ell^+}, \boldsymbol{\ell}_\perp\right)e^{i\boldsymbol{\ell}\cdot\boldsymbol{x}}\right], \tag{21}$$

$$(\hat{\ell}'-m)T^{\bar{Q}}_{i,i'}(\hat{\ell}-m) = 2\pi\int d^2\boldsymbol{x}[U^\dagger(\boldsymbol{x})-1]_{i',i}\sum_h\left[v_h\left(\ell^+, \frac{(\boldsymbol{\ell}'_\perp)^2+m^2}{2\ell^+}, \quad \boldsymbol{\ell}'_\perp\right)e^{-i\boldsymbol{\ell}'\cdot\boldsymbol{x}}\right]\left[\bar{v}_h\left(\ell^+, \frac{\boldsymbol{\ell}_\perp^2+m^2}{2\ell^+}, \boldsymbol{\ell}_\perp\right)e^{i\boldsymbol{\ell}\cdot\boldsymbol{x}}\right], \tag{22}$$

where the dummy integration variable $\boldsymbol{x}$ is the transverse coordinate of the parton, and the arguments of the spinors $u_h, v_h, \bar{u}_h, \bar{v}_h$ show explicitly the light-cone components of the corresponding partons. This result can be used in order to demonstrate that in the mixed light-cone representation in terms of the coordinates $(\ell^+, \boldsymbol{x})$, the interaction with the shock wave merely reduces to multiplication by the factor $[U(\boldsymbol{x})-1]$ for quarks and $[U^\dagger(\boldsymbol{x})-1]$ for antiquarks, as expected in the eikonal picture. It is possible to repeat this analysis for the gluonic field, analyzing a convolution $\Pi^{ac}_{\mu\alpha}(\ell)T^{g,\alpha,\beta}_{c,d}\Pi^{db}_{\beta\nu}(\ell')$, where $\Pi^{ab}_{\mu\nu}$ is the light-cone propagator taken in the Feynman or the light-cone gauge $A\cdot n = 0$. It is straightforward to show that in the light-cone representation, the interaction of the gluon with the shock wave reduces to multiplication by the factor $[\mathcal{U}^{\mathrm{sgn}(\ell^+)}(\boldsymbol{x})-1]_{b,a}$, where $\boldsymbol{x}$ is the correspondent transverse coordinate of the gluon.

C. Charmonia-bottomonia production via single-parton scattering

The single gluon in the initial state may produce heavy charmonia-bottomonia pairs via two complementary mechanisms, a hadronization of $\bar{Q}Q$ pairs into final-state quarkonia (which is described in NRQCD framework) and the fragmentation mechanism, when each of the heavy quarkonia stems from fragmentation of only one heavy (bottom) quark. The two mechanisms have completely different final states and different underlying dynamics, and for this reason will be disregarded in what follows.

1. Production of quarkonia via $\bar{Q}Q$ fusion

The charmonia-bottomonia pair production via single-parton scattering proceeds via emission of the single gluon from the projectile and subsequent formation of the heavy quarks in the field of the shock wave (gluonic field of the target). The corresponding cross section is given by

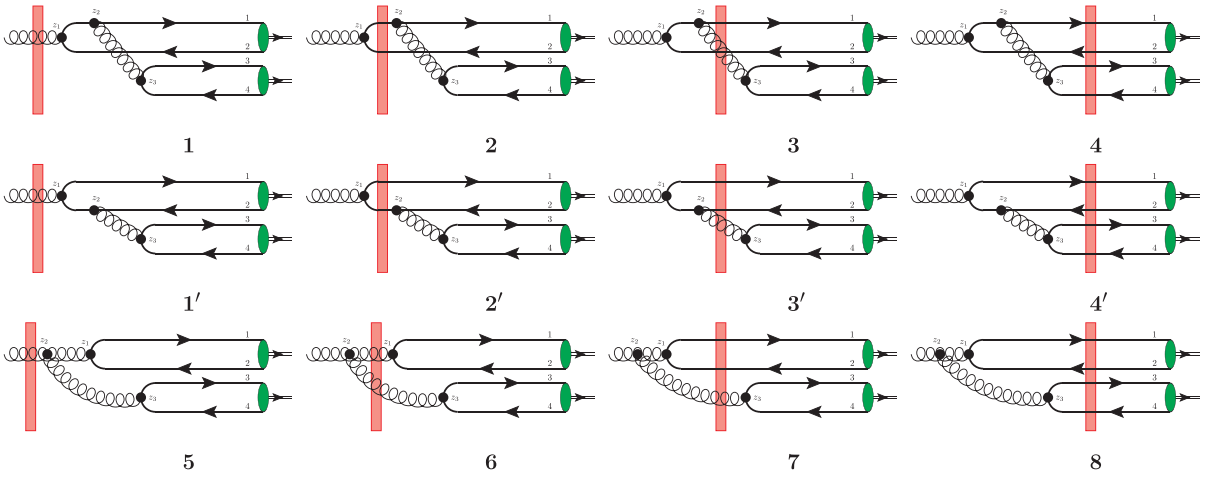


FIG. 3. Diagrams describing the inclusive charmonia-bottomonia pair production in the CGC picture in the leading order over α_s. The diagrams 1'–4' in the middle row are charge conjugate of the diagrams in the upper row (differ by inversion of the upper quark loop). The diagrams in the first three columns require formation of the (lower) quarkonium from the color octet $\bar{Q}Q$ (formed via $g \to \bar{Q}Q$ subprocess), and for this reason are suppressed by a small color octet LDME. The dominant color singlet contribution comes from the diagrams in the last row (diagrams 4, 4', and 8, respectively). The subscript numbers 1–4 in the right part of each diagram enumerate the heavy quark lines in our convention. The subscript letters $z_1 \ldots z_3$ stand for the coordinates of the interaction vertices in the configuration space. The red block represents the interaction with the target (shock wave).

$$\frac{d\sigma(p+p \to M_1+M_2+X)}{dy_1 d^2\boldsymbol{p}_1^\perp dy_2 d^2\boldsymbol{p}_2^\perp} = x_1 g(x_1) \frac{d\sigma(g+p \to M_1+M_2+X)}{dy_1 d^2\boldsymbol{p}_1^\perp dy_2 d^2\boldsymbol{p}_2^\perp}, \qquad (23)$$

where $x_1 g(x_1)$ is the standard forward gluon parton distribution function of the projectile, and $x_1 = q^+/p^+_{\text{projectile}}$ is the fraction of the projectile's light-cone "+" momentum carried by the gluon. In what follows, we will focus on the evaluation of the second term in Eq. (23), which in the leading order in strong coupling α_s obtains contributions from a set of diagrams shown in Fig. 3. We may observe that the diagrams shown in the first three columns lead to formation of one of the $\bar{Q}Q$ pairs (in inferior part of the diagram) in the color octet state. Formally, the S-wave color octet LDMEs are suppressed compared to color singlet LDMEs as $\sim\mathcal{O}(v^4)$, where $v \sim \mathcal{O}(\alpha_s(m_Q))$ is the relative velocity of the internal motion of heavy quarks inside the quarkonium, and numerically the color octet LDMEs

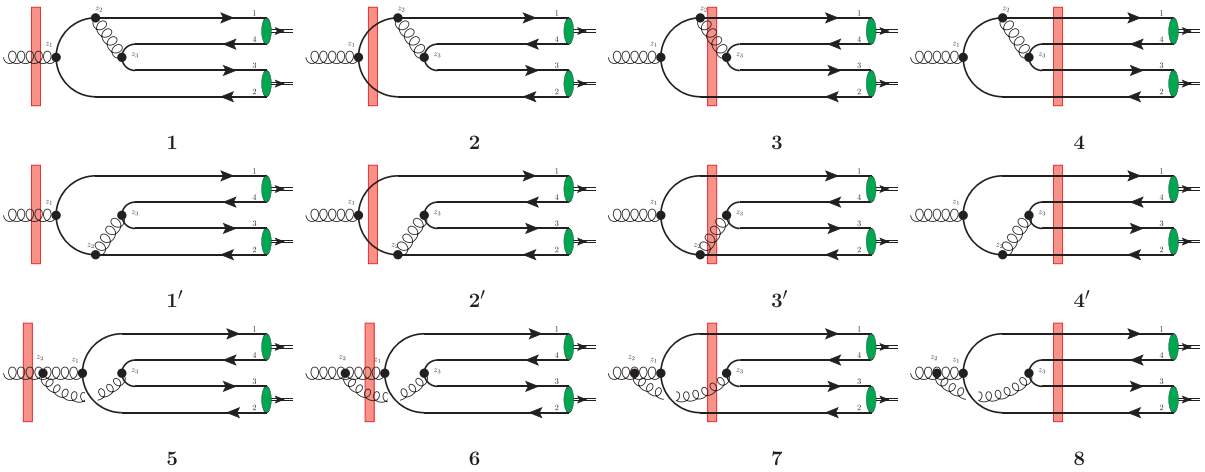


FIG. 4. Additional diagrams which in general should be taken into account for inclusive quarkonia pair production in the CGC picture in the leading order over α_s, yet do not contribute to charmonia-bottomonia pairs. The diagrams 1–4 in the upper and middle rows are related by charge conjugation (inverted direction of the quark lines). The diagrams in the first column can proceed only via color octet LDMEs and thus are suppressed. The subscript numbers 1–4 enumerate the heavy quark lines in our convention. The subscript letters $z_1 \ldots z_3$ stand for the coordinates of the interaction vertices in the configuration space. The red block represents the interaction with the target (shock wave).

indeed are very small [53,54]. For this reason, in what follows we may safely disregard these contributions and focus on evaluation of the diagrams in the last column. Furthermore, since the shock wave implies exchange of the vacuum quantum numbers in t-channel, and gluon has spin-1, the diagrams in the lower row can contribute only if both produced quarkonia have vector quantum numbers ($J^P = 1^-$). For comparison, the production of quarkonia pairs in general case requires inclusion of additional Feynman diagrams shown in Fig. 4, or emission of additional hard gluons, leading to significantly more complicated expressions for the cross sections.

In view of the expected smallness of the cross section, in what follows we will focus on the kinematics of small transverse momenta p_T, where most of the quarkonia pairs are produced. In these kinematics, we may safely disregard the diagrams in which the quarkonia formation occurs from color octet quark-antiquark pair and thus is controlled by small color octet LDMEs (diagrams 1–3, 1'–3', and 5–7 in Fig. 3). For the remaining diagrams, 4, 4', 8, the corresponding contribution in the eikonal picture can be described by a convolution of the so-called perturbative impact factors with target-dependent correlators of multipole matrix elements. The formation of the final-state quarkonia with spin S and spin projection S_z from the $\bar{Q}Q$ is described by the conventional NRQCD projectors [1–5], as follows:

$$\begin{aligned}\Pi_M^{SS_Z}(p_M,k) &= \sqrt{\frac{\langle \mathcal{O}_M\rangle}{m}}\sum_{s,\bar{s}}\left\langle \frac{1}{2}s,\frac{1}{2}\bar{s}\middle| S,S_z\right\rangle v_{\bar{s}}\left(p_M-\frac{k}{2}\right)\bar{u}_s\left(p_M+\frac{k}{2}\right)\\ &= \sqrt{\frac{\langle \mathcal{O}_M\rangle}{8m^3}}\begin{cases}\left(\frac{\hat{p}_M}{2}-\hat{k}-m\right)\gamma_5\left(\frac{\hat{p}_M}{2}+\hat{k}+m\right), & S=0\\ \left(\frac{\hat{p}_M}{2}-\hat{k}-m\right)\hat{\varepsilon}^*(p_M,S_Z)\left(\frac{\hat{p}_M}{2}+\hat{k}+m\right), & S=1,\end{cases}\end{aligned} \tag{24}$$

where $\langle \mathcal{O}_M\rangle$ are the corresponding LDMEs, and $\varepsilon^\mu(p_M)$ is the polarization vector of the produced vector quarkonium which satisfies orthogonality condition $\varepsilon\cdot p_M = 0$. From now on, we will use the notation m for the quark mass, and, in order to avoid confusion, will tacitly replace it with m_1 and m_2 in expressions where both quarks contribute. The momentum k, which describes the internal motion of the quarks in the quarkonium, can be disregarded in the heavy quark mass limit, tacitly assuming that $k = 0$ everywhere in what follows. The evaluation of the remaining diagrams is straightforward in the mixed (light-cone) representation introduced earlier. Using conventional CGC rules for the vertices, we may obtain for the amplitudes of processes shown in the diagrams 4, 4', and 8

$$\mathcal{A}_4^{(a)} = \int\prod_{n=1}^4 (d^2\boldsymbol{x}_n)e^{-i\boldsymbol{p}_1\cdot(\boldsymbol{x}_1+\boldsymbol{x}_2)/2}e^{-i\boldsymbol{p}_2\cdot(\boldsymbol{x}_3+\boldsymbol{x}_4)/2}R_4(\boldsymbol{x}_1,\boldsymbol{x}_2,\boldsymbol{x}_3,\boldsymbol{x}_4)T_a^{(4)}(\boldsymbol{x}_1,\boldsymbol{x}_2,\boldsymbol{x}_3,\boldsymbol{x}_4) \tag{25}$$

$$\mathcal{A}_{4'}^{(a)} = \int\prod_{n=1}^4 (d^2\boldsymbol{x}_n)e^{-i\boldsymbol{p}_1\cdot(\boldsymbol{x}_1+\boldsymbol{x}_2)/2}e^{-i\boldsymbol{p}_2\cdot(\boldsymbol{x}_3+\boldsymbol{x}_4)/2}R_{4'}(\boldsymbol{x}_1,\boldsymbol{x}_2,\boldsymbol{x}_3,\boldsymbol{x}_4)T_a^{(4')}(\boldsymbol{x}_1,\boldsymbol{x}_2,\boldsymbol{x}_3,\boldsymbol{x}_4) \tag{26}$$

$$\mathcal{A}_8^{(a)} = \int\prod_{n=1}^4 (d^2\boldsymbol{x}_n)e^{-i\boldsymbol{p}_1\cdot(\boldsymbol{x}_1+\boldsymbol{x}_2)/2}e^{-i\boldsymbol{p}_2\cdot(\boldsymbol{x}_3+\boldsymbol{x}_4)/2}R_8(\boldsymbol{x}_1,\boldsymbol{x}_2,\boldsymbol{x}_3,\boldsymbol{x}_4)T_a^{(8)}(\boldsymbol{x}_1,\boldsymbol{x}_2,\boldsymbol{x}_3,\boldsymbol{x}_4), \tag{27}$$

where a is the color index of the incoming gluon, R_4, R_4', R_8 are the perturbative impact factors, and $T_a^{(4)}, T_a^{(4')}, T_a^{(8)}$ are the target-dependent (multipole) correlators of Wilson lines. Explicitly, the impact factors are given by

$$\begin{aligned}R_4(\boldsymbol{x}_1,\boldsymbol{x}_2,\boldsymbol{x}_3,\boldsymbol{x}_4) &= (ig)^3\int\prod_{n=1}^4\left(\frac{d^3\ell_n}{(2\pi)^3}e^{i\boldsymbol{\ell}_n\cdot\boldsymbol{x}_n}\right)\mathrm{tr}\left[\Pi_{M_1}^{SS_Z}(p_1,0)\gamma^+S(\ell_1)\gamma^\mu S(\ell_1-\ell_3-\ell_4)\hat{\varepsilon}(q)S(-\ell_2)\gamma_+\right]\\ &\times\Pi_{\mu\nu}(\ell_3+\ell_4)\mathrm{tr}\left[\Pi_{M_2}^{SS_Z}(p_2,0)\gamma^+S(\ell_3)\gamma^\nu S(-\ell_4)\gamma_+\right](2\pi)^3\delta^3\left(q-\sum_n\ell_n\right)\end{aligned} \tag{28}$$

$$\begin{aligned}R_{4'}(\boldsymbol{x}_1,\boldsymbol{x}_2,\boldsymbol{x}_3,\boldsymbol{x}_4) &= (ig)^3\int\prod_{n=1}^4\left(\frac{d^3\ell_n}{(2\pi)^3}e^{i\boldsymbol{\ell}_n\cdot\boldsymbol{x}_n}\right)\mathrm{tr}\left[\Pi_{M_1}^{SS_Z}(p_1,0)\gamma^+S(\ell_1)\hat{\varepsilon}(q)S(\ell_1-q)\gamma^\mu S(-\ell_2)\gamma_+\right]\\ &\times\Pi_{\mu\nu}(\ell_3+\ell_4)\mathrm{tr}\left[\Pi_{M_2}^{SS_Z}(p_2,0)\gamma^+S(\ell_3)\gamma^\nu S(-\ell_4)\gamma_+\right](2\pi)^3\delta^3\left(q-\sum_n\ell_n\right)\end{aligned} \tag{29}$$

$$R_8(\boldsymbol{x}_1,\boldsymbol{x}_2,\boldsymbol{x}_3,\boldsymbol{x}_4) = (ig)^3 \int \prod_{n=1}^{4}\left(\frac{d^3\ell_n}{(2\pi)^3}e^{i\boldsymbol{\ell}_n\cdot\boldsymbol{x}_n}\right)\epsilon^\lambda(q)V_{\lambda\alpha\beta}\Pi_{\alpha\mu}(\ell_1+\ell_2)\mathrm{tr}\left[\Pi^{SS_z}_{M_1}(p_1,0)\gamma^+ S(\ell_1)\gamma^\mu S(-\ell_2)\gamma_+\right]$$
$$\times\,\Pi_{\beta\nu}(\ell_3+\ell_4)\mathrm{tr}\left[\Pi^{SS_z}_{M_2}(p_2,0)\gamma^+ S(\ell_3)\gamma^\nu S(-\ell_4)\gamma_+\right](2\pi)^3\delta^3\Big(q-\sum_n \ell_n\Big), \tag{30}$$

where the notation tr(...) implies that the trace should be taken only over the Dirac indices, $\Pi_{\mu\nu}(\ell)$ is the color-independent part of the gluon propagator, and the momenta ℓ_a are the momenta of the quarks before interaction with the shock wave. According to CGC rules discussed in Sec. II B, the interaction with the shock wave does not change the plus component of the quark momentum, and for this reason the plus components ℓ_n^+ of the momenta are fully determined by the kinematics of the corresponding meson: they coincide with $p_1^+/2$ for $n=1,2$ and with $p_2^+/2$ for $n=3,4$. For this reason, integrals over the quark momenta include only three components, namely $d^3\ell_n = d\ell_n^- d^2\boldsymbol{\ell}_n$. The $\delta^3(\ldots)$ functions which appear in the integrands of Eqs. (28)–(30) reflect conservation of the total momentum of the partonic ensemble. The notation $V_{\lambda\alpha\beta}$ in Eq. (30) is the colorless part of the standard perturbative three-gluon vertex,

$$V_{\lambda\alpha\beta} = g^{\lambda\alpha}(q-\ell_1-\ell_2)^\beta - g^{\lambda\beta}(q-\ell_3-\ell_4)^\beta + g^{\alpha\beta}(\ell_1+\ell_2-\ell_3-\ell_4)^\lambda. \tag{31}$$

The target-dependent factors $T_a^{(4)}, T_a^{(4')}, T_a^{(8)}$ are given explicitly by

$$T_a^{(4)}(\boldsymbol{x}_1,\boldsymbol{x}_2,\boldsymbol{x}_3,\boldsymbol{x}_4) = \mathrm{tr}_c(t_a t_b U(\boldsymbol{x}_1)U^\dagger(\boldsymbol{x}_2))\mathrm{tr}_c(t_b U(\boldsymbol{x}_3)U^\dagger(\boldsymbol{x}_4)) = \frac{N_c}{2}\langle S_4^{(a)}(\boldsymbol{x}_3,\boldsymbol{x}_4,\boldsymbol{x}_1,\boldsymbol{x}_2) - S_2^{(a)}(\boldsymbol{x}_1,\boldsymbol{x}_2)S_2(\boldsymbol{x}_3,\boldsymbol{x}_4)\rangle \tag{32}$$

$$T_a^{(4')}(\boldsymbol{x}_1,\boldsymbol{x}_2,\boldsymbol{x}_3,\boldsymbol{x}_4) = \mathrm{tr}_c(t_b t_a U(\boldsymbol{x}_1)U^\dagger(\boldsymbol{x}_2))\mathrm{tr}_c(t_b U(\boldsymbol{x}_3)U^\dagger(\boldsymbol{x}_4)) = \frac{N_c}{2}\langle S_4^{(a)}(\boldsymbol{x}_1,\boldsymbol{x}_2,\boldsymbol{x}_3,\boldsymbol{x}_4) - S_2^{(a)}(\boldsymbol{x}_1,\boldsymbol{x}_2)S_2(\boldsymbol{x}_3,\boldsymbol{x}_4)\rangle \tag{33}$$

$$\begin{aligned} T_a^{(8)}(\boldsymbol{x}_1,\boldsymbol{x}_2,\boldsymbol{x}_3,\boldsymbol{x}_4) &= if_{abc}\mathrm{tr}_c(t_b U(\boldsymbol{x}_1)U^\dagger(\boldsymbol{x}_2))\mathrm{tr}_c(t_c U(\boldsymbol{x}_3)U^\dagger(\boldsymbol{x}_4)) = \frac{N_c}{2}\langle S_4^{(a)}(\boldsymbol{x}_3,\boldsymbol{x}_4,\boldsymbol{x}_1,\boldsymbol{x}_2) - S_4^{(a)}(\boldsymbol{x}_1,\boldsymbol{x}_2,\boldsymbol{x}_3,\boldsymbol{x}_4)\rangle \\ &= T_a^{(4')}(\boldsymbol{x}_1,\boldsymbol{x}_2,\boldsymbol{x}_3,\boldsymbol{x}_4) - T_a^{(4)}(\boldsymbol{x}_1,\boldsymbol{x}_2,\boldsymbol{x}_3,\boldsymbol{x}_4), \end{aligned} \tag{34}$$

where the notation $\mathrm{tr}_c(\ldots)$ implies that the trace should be taken only over the color indices, and we introduced shorthand notations

$$S_4^{(a)}(\boldsymbol{x}_1,\boldsymbol{x}_2,\boldsymbol{x}_3,\boldsymbol{x}_4) = \frac{1}{N_c}\langle \mathrm{tr}_c(t_a U(\boldsymbol{x}_1)U^\dagger(\boldsymbol{x}_2)U(\boldsymbol{x}_3)U^\dagger(\boldsymbol{x}_4))\rangle_Y, \tag{35}$$

$$S_2^{(a)}(\boldsymbol{x}_1,\boldsymbol{x}_2) = \frac{1}{N_c}\langle \mathrm{tr}_c(t_a U(\boldsymbol{x}_1)U^\dagger(\boldsymbol{x}_2))\rangle_Y. \tag{36}$$

For derivation of Eqs. (32)–(34), we used heavily the Fierz identities for Gell-Mann matrices

$$(t_b)^{c_1'}_{c_1}(t_b)^{c_2'}_{c_2} = \delta^{c_1'}_{c_2}\delta^{c_2'}_{c_1} - \frac{1}{N_c}\delta^{c_1'}_{c_1}\delta^{c_2'}_{c_2}, \qquad t_b\mathrm{tr}_c(t_b\hat{A}) = \frac{1}{2}\left[\hat{A} - \frac{\hat{\mathbf{1}}}{N_c}\mathrm{tr}(A)\right], \quad \forall A, \tag{37}$$

and rewrote if_{abc} as

$$if_{abc} \equiv 2i\mathrm{tr}[t_a(t_b t_c - t_c t_b)] \tag{38}$$

in order to obtain the results shown in the second line of Eq. (34). The relation which appears in the last line of Eq. (34) implies that the expression should be antisymmetric with respect to permutation of mesons, and indicates that it will give a numerically small contribution.

The evaluation of the impact factors $R_4, R_{4'}, R_8$ simplifies drastically using the procedure discussed at the end of Sec. II B. Replacing the propagators connected to the shock wave with

$$\frac{i\sum_h u_h(\widetilde{\ell})\bar{u}_h(\widetilde{\ell})}{\ell^2-m^2+i0}, \quad \text{and} \quad \frac{i\sum_h v_h(\widetilde{\ell})\bar{v}_h(\widetilde{\ell})}{\ell^2-m^2+i0}, \qquad \widetilde{\ell}=\left(|\ell^+|,\frac{\boldsymbol{\ell}_\perp^2+m^2}{2|\ell^+|},\boldsymbol{\ell}_\perp\right) \tag{39}$$

for quarks and antiquarks respectively, we may obtain for R_4 and $R_{4'}$ the following:

$$R_4(\boldsymbol{x}_1,\boldsymbol{x}_2,\boldsymbol{x}_3,\boldsymbol{x}_4)=(ig)^3\sum_{h_1,\ldots,h_4}\int\prod_{n=1}^{4}\left(\frac{d^3\ell_n}{(2\pi)^3}e^{i\boldsymbol{\ell}_n\cdot\boldsymbol{x}_n}\right)\Pi_{M_1}^{h_1,h_2}\Pi_{M_2}^{h_3,h_4}(2\pi)^3\delta^3\Big(q-\sum_n\ell_n\Big)$$
$$\times\left[\frac{\bar{u}_{h_1}(\tilde{\ell}_1)\gamma^\mu S(\ell_1-\ell_3-\ell_4)\hat{\varepsilon}(q)v_{h_2}(\tilde{\ell}_2)}{(\ell_1^2-m_1^2+i0)(\ell_2^2-m_1^2+i0)}\right]\Pi\mu\nu(\ell+\ell)\left[\frac{\bar{u}_{h_3}(\tilde{\ell}_3)\gamma^\nu v_{h_4}(\tilde{\ell}_4)}{(\ell_3^2-m_2^2+i0)(\ell_4^2-m_2^2+i0)}\right] \tag{40}$$

$$R_{4'}(\boldsymbol{x}_1,\boldsymbol{x}_2,\boldsymbol{x}_3,\boldsymbol{x}_4)=(ig)^3\sum_{h_1,\ldots,h_4}\int\prod_{n=1}^{4}\left(\frac{d^3\ell_n}{(2\pi)^3}e^{i\boldsymbol{\ell}_n\cdot\boldsymbol{x}_n}\right)\Pi_{M_1}^{h_1,h_2}\Pi_{M_2}^{h_3,h_4}(2\pi)^3\delta^3\Big(q-\sum_n\ell_n\Big)$$
$$\times\left[\frac{\bar{u}_{h_1}(\tilde{\ell}_1)\hat{\varepsilon}(q)S(\ell_1-q)\gamma^\mu v_{h_2}(\tilde{\ell}_2)}{(\ell_1^2-m_1^2+i0)(\ell_2^2-m_1^2+i0)}\right]\Pi_{\mu\nu}(\ell_3+\ell_4)\left[\frac{\bar{u}_{h_3}(\tilde{\ell}_3)\gamma^\nu v_{h_4}(\tilde{\ell}_4)}{(\ell_3^2-m_2^2+i0)(\ell_4^2-m_2^2+i0)}\right], \tag{41}$$

where we introduced shorthand notations

$$\bar{\Pi}_{M_1}^{h_1,h_2}=\bar{v}_{h_2}(\widetilde{\ell}_2)\gamma_+\Pi_{M_1}^{SS_Z}(p_1,0)\gamma^+u_{h_1}(\widetilde{\ell}_1), \tag{42}$$

$$\bar{\Pi}_{M_2}^{h_3,h_4}=\bar{v}_{h_4}(\widetilde{\ell}_4)\gamma_+\Pi_{M_2}^{SS_Z}(p_2,0)\gamma^+u_{h_3}(\widetilde{\ell}_3). \tag{43}$$

As we will show now, the matrices $\bar{\Pi}_{M_1}^{h_1,h_2},\bar{\Pi}_{M_2}^{h_3,h_4}$ do not depend on the integration momenta ℓ_n. In order to demonstrate this, we will rewrite the explicit form of the NRQCD projectors (24) as

$$\Pi_M^{SS_Z}(p_M,0)=\left(\frac{\hat{p}_M}{2}-m\right)\Gamma_M\left(\frac{\hat{p}_M}{2}+m\right)=\sum_{h,\bar{h}}v_{\bar{h}}\Big(\frac{p_M}{2}\Big)\bar{v}_{\bar{h}}\Big(\frac{p_M}{2}\Big)\Gamma_M u_h\Big(\frac{p_M}{2}\Big)\bar{u}_h\Big(\frac{p_M}{2}\Big), \tag{44}$$

where Γ_M is the appropriate (spin/helicity dependent) Dirac matrix multiplied by the corresponding LDME. Substituting Eq. (44) into Eqs. (42) and (43), we may obtain for the NRQCD projectors in helicity basis

$$\bar{\Pi}_M^{h_1,h_2}=\bar{v}_{h_2}(\widetilde{\ell}_2)\gamma_+\left(\sum_{h,\bar{h}}v_{\bar{h}}\Big(\frac{p_M}{2}\Big)\bar{v}_{\bar{h}}\Big(\frac{p_M}{2}\Big)\Gamma_M u_h\Big(\frac{p_M}{2}\Big)\bar{u}_h\Big(\frac{p_M}{2}\Big)\right)\gamma^+u_{h_1}(\widetilde{\ell}_1)=(p_M^+)^2\bar{v}_{h_2}\Big(\frac{p_M}{2}\Big)\Gamma_M u_{h_1}\Big(\frac{p_M}{2}\Big), \tag{45}$$

where we used identities for the light-cone spinors $\bar{v}_{h_1}(p)\gamma_+v_{h_2}(q)=\bar{u}_{h_1}(p)\gamma_+u_{h_2}(q)=2\delta_{h_1,h_2}\sqrt{p^+q^+}$ [10], as well as $\widetilde{\ell}_1^+=\widetilde{\ell}_2^+=p_M^+/2$, which is a consequence of the fact that shock wave does not change the "+" momentum of the parton. The structure of Eqs. (40) and (41) demonstrates that the impact factors essentially reduce to a convolution of the light-cone wave functions with NRQCD projectors in helicity basis. Indeed, if we express ℓ_2 in terms of the other light-cone momenta and take the integrals over ℓ_1^-,ℓ_3^- using identities based on the Cauchy theorem, as follows:

$$\int_{-\infty}^{+\infty}\frac{d\ell_1^-}{2\pi}\frac{1}{(2\ell_1^+\ell_1^--\boldsymbol{\ell}_{1,\perp}^2-m_1^2+i0)(2(k^++\ell_1^+)(k^-+\ell_1^-)-(\boldsymbol{k}_\perp+\boldsymbol{\ell}_{1,\perp})^2-m_1^2+i0)}$$
$$\times\frac{1}{(2(q^+-k^+-\ell_1^+)(q^--k^--\ell_1^-)-(\boldsymbol{k}+\boldsymbol{\ell}_{1,\perp})^2-m_1^2+i0)}$$
$$=\frac{i\Theta(q^+-k^+-\ell_1^+)}{8\ell_1^+(\ell_1^++k^+)(q^+-k^+-\ell_1^+)\left[-\frac{q^+(\boldsymbol{\ell}_{1,\perp}^2+m_1^2)}{2(q^+-k^+-\ell_1^+)(k^++\ell_1^+)}\right]\left[-\frac{\boldsymbol{k}_\perp^2}{2k^+}-\frac{\boldsymbol{\ell}_{1\perp}^2+m_1^2}{2\ell_0^+}-\frac{(\boldsymbol{k}_\perp+\boldsymbol{\ell}_{1\perp})^2+m_1^2}{2(q^+-k^+-\ell_1^+)}\right]}, \tag{46}$$

$$\int_{-\infty}^{+\infty}\frac{d\ell_1^-}{2\pi}\frac{(k^-+\ell_1^-)}{(2\ell_1^+\ell_1^- - \boldsymbol{\ell}_{1\perp}^2 - m_1^2+i0)(2(k^++\ell_1^+)(k^-+\ell_1^-)-(\boldsymbol{k}_\perp+\boldsymbol{\ell}_{1\perp})^2-m_1^2+i0)}$$
$$\times\frac{1}{(2(q^+-k^+-\ell_1^+)(q^--k^--\ell_1^-)-(\boldsymbol{k}_\perp+\boldsymbol{\ell}_{1\perp})^2-m_1^2+i0)}$$
$$=\frac{i\Theta(q^+-k^+-\ell_1^+)\,\frac{(\boldsymbol{k}_\perp+\boldsymbol{\ell}_{1\perp})^2+m_1^2}{2(k^++\ell_1^+)}}{8\ell_1^+(\ell_1^++k^+)(q^+-k^+-\ell_1^+)\left[q^- - \frac{q^+(\boldsymbol{\ell}_{1\perp}^2+m_1^2)}{2(q^+-k^+-\ell_1^+)(k^++\ell_1^+)}\right]\left[q^- - \frac{\boldsymbol{k}_\perp^2}{2k^+} - \frac{\boldsymbol{\ell}_{1\perp}^2+m_1^2}{2\ell_1^+} - \frac{(\boldsymbol{k}_\perp+\boldsymbol{\ell}_{1\perp})^2+m_1^2}{2(q^+-k^+-\ell_1^+)}\right]}$$
$$+\frac{i\Theta(q^+-k^+-\ell_1^+)}{8\ell_1^+(\ell_1^++k^+)(q^+-k^+-\ell_1^+)\left[q^- - \frac{\boldsymbol{k}_\perp^2}{2k^+} - \frac{\boldsymbol{\ell}_{1\perp}^2+m_1^2}{2\ell_1^+} - \frac{(\boldsymbol{k}_\perp+\boldsymbol{\ell}_{1\perp})^2+m_1^2}{2(q^+-k^+-\ell_1^+)}\right]}, \tag{47}$$

$$\int_{-\infty}^{+\infty}\frac{d\ell_3^-}{2\pi}\frac{1}{(2\ell_3^+\ell_3^- - \boldsymbol{\ell}_{3\perp}^2 - m_2^2+i0)(2(k^+-\ell_3^+)(k^--\ell_3^-)-(\boldsymbol{k}_\perp-\boldsymbol{\ell}_{3\perp})^2-m_2^2+i0)}$$
$$=\frac{\Theta(k^+-\ell_3^+)}{4\ell_3^+(k^+-\ell_3^+)}\frac{i}{k^- - \frac{\boldsymbol{\ell}_{3\perp}^2+m^2}{2\ell_3^+} - \frac{(\boldsymbol{k}_\perp-\boldsymbol{\ell}_{3\perp})^2+m_2^2}{2(k^+-\ell_3^+)}}, \tag{48}$$

where $k=\ell_3+\ell_4$, we recover the light-cone energy denominators, which should appear in diagram 4 according to the light-cone perturbation theory suggested long ago in Refs. [10,48]. Similarly, if we express ℓ_1 in terms of ℓ_2, k and apply identities (46) and (47) with permuted dummy integration variable $\ell_1^- \to \ell_2^-$, we will recover the light-cone energy denominators for the diagram 4′. The remaining integration over the transverse components is straightforward and allows us to express the impact factors as convolutions, as follows:

$$R_4(\boldsymbol{x}_1,\boldsymbol{x}_2,\boldsymbol{x}_3,\boldsymbol{x}_4)=\sum_{h_1,\ldots,h_4}\bar{\Pi}_{M_1}^{h_1,h_2}\bar{\Pi}_{M_2}^{h_3,h_4}A_{h_1,h_2,h_3,h_4}(\{\alpha_i,\boldsymbol{x}_i\})e^{-i\boldsymbol{p}_1\cdot(\boldsymbol{x}_1+\boldsymbol{x}_2)/2}e^{-i\boldsymbol{p}_2\cdot(\boldsymbol{x}_3+\boldsymbol{x}_4)/2} \tag{49}$$

$$R_{4'}(\boldsymbol{x}_1,\boldsymbol{x}_2,\boldsymbol{x}_3,\boldsymbol{x}_4)=\sum_{h_1,\ldots,h_4}\bar{\Pi}_{M_1}^{h_1,h_2}\bar{\Pi}_{M_2}^{h_3,h_4}B_{h_1,h_2,h_3,h_4}(\{\alpha_i,\boldsymbol{x}_i\})e^{-i\boldsymbol{p}_1\cdot(\boldsymbol{x}_1+\boldsymbol{x}_2)/2}e^{-i\boldsymbol{p}_2\cdot(\boldsymbol{x}_3+\boldsymbol{x}_4)/2}\times \tag{50}$$

where the functions $A_{h_1,h_2,h_3,h_4}, B_{h_1,h_2,h_3,h_4}$ are defined as

$$A_{h_1,h_2,h_3,h_4}(\{\alpha_i,\boldsymbol{x}_i\})=e^{i\boldsymbol{p}_1\cdot(\boldsymbol{x}_1+\boldsymbol{x}_2)/2}e^{i\boldsymbol{p}_2\cdot(\boldsymbol{x}_3+\boldsymbol{x}_4)/2}\sum_{h_1,\ldots,h_4}\int\prod_{n=1}^{4}\left(\frac{d^3\ell_n}{(2\pi)^3}e^{i\boldsymbol{\ell}_n\cdot\boldsymbol{x}_n}\right)(2\pi)^3\delta^3\left(q-\sum_n\ell_n\right)$$
$$\times(ig)^3\left[\frac{\bar{u}_{h_1}(\tilde{\ell}_1)\gamma^\mu S(\ell_1-\ell_3-\ell_4)\hat{\epsilon}(q)v_{h_2}(\tilde{\ell}_2)}{(\ell_1^2-m_1^2+i0)(\ell_2^2-m_1^2+i0)}\right]\Pi\mu\nu(\ell_3+\ell_4)\left[\frac{\bar{u}_{h_3}(\tilde{\ell}_3)\gamma^\nu v_{h_4}(\tilde{\ell}_4)}{(\ell_3^2-m_2^2+i0)(\ell_4^2-m_2^2+i0)}\right] \tag{51}$$

$$B_{h_1,h_2,h_3,h_4}(\{\alpha_i,\boldsymbol{x}_i\})=e^{i\boldsymbol{p}_1\cdot(\boldsymbol{x}_1+\boldsymbol{x}_2)/2}e^{i\boldsymbol{p}_2\cdot(\boldsymbol{x}_3+\boldsymbol{x}_4)/2}\int\prod_{n=1}^{4}\left(\frac{d^3\ell_n}{(2\pi)^3}e^{i\boldsymbol{\ell}_n\cdot\boldsymbol{x}_n}\right)(2\pi)^3\delta^3\left(q-\sum_n\ell_n\right)$$
$$\times(ig)^3\left[\frac{\bar{u}_{h_1}(\tilde{\ell}_1)\hat{\epsilon}(q)S(\ell_1-q)\gamma^\mu v_{h_2}(\tilde{\ell}_2)}{(\ell_1^2-m_1^2+i0)(\ell_2^2-m_1^2+i0)}\right]\Pi_{\mu\nu}(\ell_3+\ell_4)\left[\frac{\bar{u}_{h_3}(\tilde{\ell}_3)\gamma^\nu v_{h_4}(\tilde{\ell}_4)}{(\ell_3^2-m_2^2+i0)(\ell_4^2-m_2^2+i0)}\right]$$
$$=-A_{h_2,h_1,h_4,h_3}(\alpha_2,\boldsymbol{x}_2,\alpha_1,\boldsymbol{x}_1,\alpha_4,\boldsymbol{x}_4,\alpha_3,\boldsymbol{x}_3) \tag{52}$$

and the corresponding light-cone fractions α_i in the heavy quark mass limit are given by

$$\alpha_1=\alpha_2=\frac{p_{M_1}^+}{2q^+},\qquad \alpha_3=\alpha_4=\frac{p_{M_1}^+}{2q^+}. \tag{53}$$

The evaluation of the expressions for $A_{h_1,h_2,h_3,h_4}, B_{h_1,h_2,h_3,h_4}$ essentially coincides with the light-cone wave functions of the $\bar{Q}Q\bar{Q}Q$ Fock state in the photon (namely, the partonic amplitude $\gamma\to\bar{Q}Q\bar{Q}Q$), which was done in Ref. [55], and after several algebraic simplifications may be reduced to the form

$$
\begin{aligned}
A(\{\alpha_i,\boldsymbol{r}_i\}) = &-\frac{2\sqrt{4\pi\alpha_s(\mu)}\alpha_s(\mu)}{\pi^3(1-\alpha_1-\alpha_2)^2\sqrt{\alpha_1\alpha_2}}\int\frac{q_1dq_1k_2dk_2}{\frac{\bar\alpha_2q_1^2}{\alpha_1(1-\alpha_1-\alpha_2)}+\frac{m_1^2(\alpha_1+\alpha_2)}{\alpha_1\alpha_2}+\frac{k_2^2}{\alpha_2\bar\alpha_2}}\\
&\times\frac{1}{k_2^2+m_1^2}\sqrt{\frac{\alpha_2}{\alpha_1}}\Big[(\alpha_2\delta_{\gamma,a_2}-\bar\alpha_2\delta_{\gamma,-a_2})(\bar\alpha_2\delta_{\lambda,a_1}+\alpha_1\delta_{\lambda,-a_1})\delta_{a_1,-a_2}\\
&\times(\boldsymbol{n}_{2,134}\cdot\boldsymbol{\varepsilon}_\gamma)(\boldsymbol{n}_{1,34}\cdot\boldsymbol{\varepsilon}_\lambda^*)k_2J_1(k_2|\boldsymbol{x}_2-\boldsymbol{b}_{134}|)q_1J_1(q_1|\boldsymbol{x}_1-\boldsymbol{b}_{34}|)\\
&+\frac{m_q^2}{2}\delta_{\lambda,-a_1}\delta_{\gamma,a_2}\delta_{a_1,-a_2}J_0(k_2|\boldsymbol{x}_2-\boldsymbol{b}_{134}|)J_0(q_1|\boldsymbol{x}_1-\boldsymbol{b}_{34}|)\frac{(1-\alpha_1-\alpha_2)^2}{1-\alpha_2}\\
&-\frac{im_q}{\sqrt{2}}\mathrm{sign}(a_2)\delta_{\gamma,a_2}\delta_{a_1,a_2}(\bar\alpha_2\delta_{\lambda,a_1}+\alpha_1\delta_{\lambda,-a_1})\boldsymbol{n}_{1,34}\cdot\boldsymbol{\varepsilon}_\lambda^*q_1J_1(q_1|\boldsymbol{x}_1-\boldsymbol{b}_{34}|)J_0(k_2|\boldsymbol{x}_2-\boldsymbol{b}_{134}|)\\
&-\frac{im_q}{\sqrt{2}}\mathrm{sign}(a_1)\delta_{\lambda,-a_1}(\alpha_2\delta_{\gamma,a_2}-\bar\alpha_2\delta_{\gamma,-a_2})\delta_{a_1,a_2}\frac{(1-\alpha_1-\alpha_2)^2}{1-\alpha_2}(\boldsymbol{n}_{2,134}\cdot\boldsymbol{\varepsilon}_\gamma)k_2J_1(k_2|\boldsymbol{x}_2-\boldsymbol{b}_{134}|)J_0(q_1|\boldsymbol{x}_1-\boldsymbol{b}_{34}|)\Big]\\
&\times\Psi^{-\lambda}_{a_3,a_4}\left(\frac{\alpha_3}{\alpha_3+\alpha_4},\boldsymbol{r}_{34},m_2,\sqrt{m_2^2+\frac{\alpha_3\alpha_4}{\alpha_3+\alpha_4}\left[\frac{\bar\alpha_2q_1^2}{\alpha_1(1-\alpha_1-\alpha_2)}+\frac{m_1^2(\alpha_1+\alpha_2)}{\alpha_1\alpha_2}+\frac{k_2^2}{\alpha_2\bar\alpha_2}\right]}\right),
\end{aligned}
\tag{54}
$$

where

$$
\Psi^\lambda_{h\bar h}(z,\boldsymbol{r}_{12},m_q,a)=-\frac{2}{(2\pi)}\left[(z\delta_{\lambda,h}-(1-z)\delta_{\lambda,-h})\delta_{h,-\bar h}i\boldsymbol{\varepsilon}_\lambda\cdot\nabla-\frac{m_q}{\sqrt{2}}\mathrm{sign}(h)\delta_{\lambda,h}\delta_{h,\bar h}\right]K_0(a\boldsymbol{r}).
\tag{55}
$$

For the impact factor of R_8, we may repeat the same analysis and replace propagators of the partons which cross the shock wave with Eq. (39). After some algebraic simplifications, we may get a structure similar to Eqs. (49) and (50), namely

$$
R_8(\boldsymbol{x}_1,\boldsymbol{x}_2,\boldsymbol{x}_3,\boldsymbol{x}_4)=\sum_{h_1,\ldots,h_4}\bar\Pi_{M_1}^{h_1,h_2}\bar\Pi_{M_2}^{h_3,h_4}C_{h_1,h_2,h_3,h_4}(\{\alpha_i,\boldsymbol{x}_i\})e^{-i\boldsymbol{p}_1\cdot(\boldsymbol{x}_1+\boldsymbol{x}_2)/2}e^{-i\boldsymbol{p}_2\cdot(\boldsymbol{x}_3+\boldsymbol{x}_4)/2},
\tag{56}
$$

where the function C_{h_1,h_2,h_3,h_4} is defined as

$$
\begin{aligned}
C_{h_1,h_2,h_3,h_4}(\{\alpha_i,\boldsymbol{x}_i\}) = &\,e^{i\boldsymbol{p}_1\cdot(\boldsymbol{x}_1+\boldsymbol{x}_2)/2}e^{i\boldsymbol{p}_2\cdot(\boldsymbol{x}_3+\boldsymbol{x}_4)/2}(ig)^3\int\prod_{n=1}^4\left(\frac{d^3\ell_n}{(2\pi)^3}e^{i\boldsymbol{\ell}_n\cdot\boldsymbol{x}_n}\right)\varepsilon^\lambda(q)V_{\lambda\alpha\beta}\\
&\times\Pi_{\alpha\mu}(\ell_1+\ell_2)\left[\frac{\bar u_{h_1}(\tilde\ell_1)\gamma^\mu v_{h_2}(\tilde\ell_2)}{(\ell_1^2-m_1^2+i0)(\ell_2^2-m_1^2+i0)}\right]\Pi_{\beta\nu}(\ell_3+\ell_4)\left[\frac{\bar u_{h_3}(\tilde\ell_3)\gamma^\nu v_{h_4}(\tilde\ell_4)}{(\ell_3^2-m_2^2+i0)(\ell_4^2-m_2^2+i0)}\right]\\
&\times(2\pi)^3\delta^3\Big(q-\sum_n\ell_n\Big)
\end{aligned}
\tag{57}
$$

and is antisymmetric with respect to permutation of pairs of the final-state quarks $(12)\leftrightarrow(34)$. The expressions in the square brackets of the second line of Eq. (57) clearly coincide with the wave functions of $\gamma\to\bar QQ$ in the momentum space [56]; for this reason, the function $C_{h_1,h_2,h_3,h_4}(\{\alpha_i,\boldsymbol{x}_i\})$ in light-cone representation can be represented as a product of the wave functions $\Psi^\lambda_{h_1,h_2}(\boldsymbol{r}_{12},m_1)$, $\Psi^\lambda_{h_3,h_4}(\boldsymbol{r}_{34},m_2)$ defined in Eq. (55) convoluted with gluon propagators. Summarizing our findings, we may rewrite the amplitude of the $g\to M_1M_2X$ subprocess as

$$
\begin{aligned}
\mathcal{A}_a(p_1,S_1;p_2,S_2) = &\,\bar\Pi_{M_1}^{h_1,h_2}\bar\Pi_{M_2}^{h_3,h_4}\int\prod_{n=1}^4(d^2\boldsymbol{x}_n)e^{-i\boldsymbol{p}_1\cdot(\boldsymbol{x}_1+\boldsymbol{x}_2)/2}e^{-i\boldsymbol{p}_2\cdot(\boldsymbol{x}_3+\boldsymbol{x}_4)/2}\\
&\times[\bar A_{h_1,h_2,h_3,h_4}(\{\alpha_i,\boldsymbol{x}_i\})T_a^{(4)}(\boldsymbol{x}_1,\boldsymbol{x}_2,\boldsymbol{x}_3,\boldsymbol{x}_4)+\bar B_{h_1,h_2,h_3,h_4}(\{\alpha_i,\boldsymbol{x}_i\})T_a^{(4')}(\boldsymbol{x}_1,\boldsymbol{x}_2,\boldsymbol{x}_3,\boldsymbol{x}_4)],
\end{aligned}
\tag{58}
$$

where we defined shorthand notations

$$
\bar A_{a_1,a_2,a_3,a_4}(\{\alpha_i,\boldsymbol{x}_i\})=A_{a_1,a_2,a_3,a_4}(\{\alpha_i,\boldsymbol{x}_i\})-C_{a_1,a_2,a_3,a_4}(\{\alpha_i,\boldsymbol{x}_i\}),
\tag{59}
$$

$$\bar{B}_{a_1,a_2,a_3,a_4}(\{\alpha_i,\boldsymbol{x}_i\}) = B_{a_1,a_2,a_3,a_4}(\{\alpha_i,\boldsymbol{x}_i\}) + C_{a_1,a_2,a_3,a_4}(\{\alpha_i,\boldsymbol{x}_i\}), \tag{60}$$

and used the last two identities in Eq. (34) for simplifications. In the inclusive cross section, we have to average (integrate over the color sources) the square of the amplitude $|\mathcal{A}_a|^2$, which requires evaluation of the convolutions of different elements $S_{2n}^{(a)}$; for the latter we can use an identity

$$S_{2n}^{(b)}(\boldsymbol{x}_1,\ldots,\boldsymbol{x}_{2n})S_{2m}^{(b)}(\boldsymbol{y}_1,\ldots,\boldsymbol{y}_{2m}) = \frac{1}{2N_c}\langle S_{2n+2m}(\boldsymbol{x}_1,\ldots,\boldsymbol{x}_{2n},\boldsymbol{y}_1,\ldots,\boldsymbol{y}_{2m}) - S_{2n}(\boldsymbol{x}_1,\ldots,\boldsymbol{x}_{2n})S_{2m}(\boldsymbol{y}_1,\ldots,\boldsymbol{y}_{2m})\rangle, \tag{61}$$

which also follows from Eq. (37). The final result of this procedure is

$$\begin{aligned}
\frac{d\sigma(g+p\to M_1+M_2+X)}{dy_1 d^2\boldsymbol{p}_1^\perp dy_2 d^2\boldsymbol{p}_2^\perp} &= \frac{1}{16\pi}|\mathcal{A}_a(p_{M_1},S_1;p_{M_2},S_2)|^2 = \frac{N_c^2}{64\pi}\int\prod_{n=1}^{4}(d^2\boldsymbol{x}_n d^2\boldsymbol{y}_n)\\
&\times e^{-i\boldsymbol{p}_1\cdot(\boldsymbol{x}_1+\boldsymbol{x}_2-\boldsymbol{y}_1-\boldsymbol{y}_2)/2}e^{-i\boldsymbol{p}_2\cdot(\boldsymbol{x}_3+\boldsymbol{x}_4-\boldsymbol{y}_3-\boldsymbol{y}_4)/2}\bar{\Pi}_{M_1}^{a_1,a_2}\bar{\Pi}_{M_2}^{a_3,a_4}\bar{\Pi}_{M_1}^{b_1,b_2*}\bar{\Pi}_{M_2}^{b_3,b_4*}\\
&\times\big[S_4(\boldsymbol{x}_1,\boldsymbol{x}_2,\boldsymbol{y}_2,\boldsymbol{y}_1)S_2(\boldsymbol{x}_4,\boldsymbol{x}_3)S_2(\boldsymbol{y}_4,\boldsymbol{y}_3)\psi_{a_1,a_2,a_3,a_4}(\{\alpha_i,\boldsymbol{x}_i\})\psi_{b_1,b_2,b_3,b_4}(\{\alpha_i,\boldsymbol{y}_i\})^*\\
&-\psi_{b_1,b_2,b_3,b_4}(\{\alpha_i,\boldsymbol{y}_i\})^*S_2(\boldsymbol{y}_4,\boldsymbol{y}_3)\\
&\times\big[\bar{A}_{a_1,a_2,a_3,a_4}S_6(\boldsymbol{x}_3,\boldsymbol{x}_4,\boldsymbol{x}_1,\boldsymbol{x}_2,\boldsymbol{y}_2,\boldsymbol{y}_1)+\bar{B}_{a_1,a_2,a_3,a_4}S_6(\boldsymbol{x}_1,\boldsymbol{x}_2,\boldsymbol{x}_3,\boldsymbol{x}_4,\boldsymbol{y}_2,\boldsymbol{y}_1)\big]\\
&-\psi_{a_1,a_2,a_3,a_4}(\{\alpha_i,\boldsymbol{x}_i\})S_2(\boldsymbol{x}_4,\boldsymbol{x}_3)\\
&\times\big[\bar{A}^*_{b_1,b_2,b_3,b_4}S_6(\boldsymbol{y}_3,\boldsymbol{y}_4,\boldsymbol{y}_1,\boldsymbol{y}_2,\boldsymbol{x}_2,\boldsymbol{x}_1)+\bar{B}^*_{b_1,b_2,b_3,b_4}S_6(\boldsymbol{y}_4,\boldsymbol{y}_3,\boldsymbol{y}_2,\boldsymbol{y}_1,\boldsymbol{x}_2,\boldsymbol{x}_1)\big]\\
&+\bar{A}_{a_1,a_2,a_3,a_4}\bar{A}^*_{b_1,b_2,b_3,b_4}S_8(\boldsymbol{x}_3,\boldsymbol{x}_4,\boldsymbol{x}_1,\boldsymbol{x}_2,\boldsymbol{y}_2,\boldsymbol{y}_1,\boldsymbol{y}_4,\boldsymbol{y}_3)\\
&+\bar{B}_{a_1,a_2,a_3,a_4}\bar{A}^*_{b_1,b_2,b_3,b_4}S_8(\boldsymbol{x}_1,\boldsymbol{x}_2,\boldsymbol{x}_3,\boldsymbol{x}_4,\boldsymbol{y}_2,\boldsymbol{y}_1,\boldsymbol{y}_4,\boldsymbol{y}_3)\\
&+\bar{A}_{a_1,a_2,a_3,a_4}\bar{B}^*_{b_1,b_2,b_3,b_4}S_8(\boldsymbol{x}_3,\boldsymbol{x}_4,\boldsymbol{x}_1,\boldsymbol{x}_2,\boldsymbol{y}_4,\boldsymbol{y}_3,\boldsymbol{y}_2,\boldsymbol{y}_1)\\
&+\bar{B}_{a_1,a_2,a_3,a_4}\bar{B}^*_{b_1,b_2,b_3,b_4}S_8(\boldsymbol{x}_1,\boldsymbol{x}_2,\boldsymbol{x}_3,\boldsymbol{x}_4,\boldsymbol{y}_4,\boldsymbol{y}_3,\boldsymbol{y}_2,\boldsymbol{y}_1)\big],
\end{aligned} \tag{62}$$

where we introduced a shorthand notation

$$\psi(\{\alpha_i,\boldsymbol{x}_i\}) = A(\{\alpha_i,\boldsymbol{x}_i\}) + B(\{\alpha_i,\boldsymbol{x}_i\}) = \bar{A}(\{\alpha_i,\boldsymbol{x}_i\}) + \bar{B}(\{\alpha_i,\boldsymbol{x}_i\}),$$

and contracted color indices of incoming gluons using identities

$$\begin{aligned}
&T_a^{(4)}(\boldsymbol{x}_1,\boldsymbol{x}_2,\boldsymbol{x}_3,\boldsymbol{x}_4)(T_a^{(4)}(\boldsymbol{y}_1,\boldsymbol{y}_2,\boldsymbol{y}_3,\boldsymbol{y}_4))^*\\
&=\frac{N_c^2}{4}[S_8(\boldsymbol{x}_3,\boldsymbol{x}_4,\boldsymbol{x}_1,\boldsymbol{x}_2,\boldsymbol{y}_2,\boldsymbol{y}_1,\boldsymbol{y}_4,\boldsymbol{y}_3)+S_4(\boldsymbol{x}_1,\boldsymbol{x}_2,\boldsymbol{y}_2,\boldsymbol{y}_1)S_2(\boldsymbol{x}_4,\boldsymbol{x}_3)S_2(\boldsymbol{y}_4,\boldsymbol{y}_3)\\
&\quad-S_6(\boldsymbol{x}_3,\boldsymbol{x}_4,\boldsymbol{x}_1,\boldsymbol{x}_2,\boldsymbol{y}_2,\boldsymbol{y}_1)S_2(\boldsymbol{y}_4,\boldsymbol{y}_3)-S_6(\boldsymbol{y}_3,\boldsymbol{y}_4,\boldsymbol{y}_1,\boldsymbol{y}_2,\boldsymbol{x}_2,\boldsymbol{x}_1)S_2(\boldsymbol{x}_4,\boldsymbol{x}_3)]
\end{aligned} \tag{63}$$

$$\begin{aligned}
&T_a^{(4')}(\boldsymbol{x}_1,\boldsymbol{x}_2,\boldsymbol{x}_3,\boldsymbol{x}_4)(T_a^{(4)}(\boldsymbol{y}_1,\boldsymbol{y}_2,\boldsymbol{y}_3,\boldsymbol{y}_4))^*\\
&=\frac{N_c^2}{4}[S_8(\boldsymbol{x}_1,\boldsymbol{x}_2,\boldsymbol{x}_3,\boldsymbol{x}_4,\boldsymbol{y}_2,\boldsymbol{y}_1,\boldsymbol{y}_4,\boldsymbol{y}_3)+S_4(\boldsymbol{x}_1,\boldsymbol{x}_2,\boldsymbol{y}_2,\boldsymbol{y}_1)S_2(\boldsymbol{x}_4,\boldsymbol{x}_3)S_2(\boldsymbol{y}_4,\boldsymbol{y}_3)\\
&\quad-S_6(\boldsymbol{x}_1,\boldsymbol{x}_2,\boldsymbol{x}_3,\boldsymbol{x}_4,\boldsymbol{y}_2,\boldsymbol{y}_1)S_2(\boldsymbol{y}_4,\boldsymbol{y}_3)-S_6(\boldsymbol{y}_3,\boldsymbol{y}_4,\boldsymbol{y}_1,\boldsymbol{y}_2,\boldsymbol{x}_2,\boldsymbol{x}_1)S_2(\boldsymbol{x}_4,\boldsymbol{x}_3)]
\end{aligned} \tag{64}$$

$$\begin{aligned}
&T_a^{(4)}(\boldsymbol{x}_1,\boldsymbol{x}_2,\boldsymbol{x}_3,\boldsymbol{x}_4)(T_a^{(4')}(\boldsymbol{y}_1,\boldsymbol{y}_2,\boldsymbol{y}_3,\boldsymbol{y}_4))^*\\
&=\frac{N_c^2}{4}[S_8(\boldsymbol{x}_3,\boldsymbol{x}_4,\boldsymbol{x}_1,\boldsymbol{x}_2,\boldsymbol{y}_4,\boldsymbol{y}_3,\boldsymbol{y}_2,\boldsymbol{y}_1)+S_4(\boldsymbol{x}_1,\boldsymbol{x}_2,\boldsymbol{y}_2,\boldsymbol{y}_1)S_2(\boldsymbol{x}_4,\boldsymbol{x}_3)S_2(\boldsymbol{y}_4,\boldsymbol{y}_3)\\
&\quad-S_6(\boldsymbol{x}_3,\boldsymbol{x}_4,\boldsymbol{x}_1,\boldsymbol{x}_2,\boldsymbol{y}_2,\boldsymbol{y}_1)S_2(\boldsymbol{y}_4,\boldsymbol{y}_3)-S_6(\boldsymbol{y}_4,\boldsymbol{y}_3,\boldsymbol{y}_2,\boldsymbol{y}_1,\boldsymbol{x}_2,\boldsymbol{x}_1)S_2(\boldsymbol{x}_4,\boldsymbol{x}_3)]
\end{aligned} \tag{65}$$

$$T_a^{(4')}(\boldsymbol{x}_1,\boldsymbol{x}_2,\boldsymbol{x}_3,\boldsymbol{x}_4)(T_a^{(4')}(\boldsymbol{y}_1,\boldsymbol{y}_2,\boldsymbol{y}_3,\boldsymbol{y}_4))^* = \frac{N_c^2}{4}[S_8(\boldsymbol{x}_1,\boldsymbol{x}_2,\boldsymbol{x}_3,\boldsymbol{x}_4,\boldsymbol{y}_4,\boldsymbol{y}_3,\boldsymbol{y}_2,\boldsymbol{y}_1) + S_4(\boldsymbol{x}_1,\boldsymbol{x}_2,\boldsymbol{y}_2,\boldsymbol{y}_1)S_2(\boldsymbol{x}_4,\boldsymbol{x}_3)S_2(\boldsymbol{y}_4,\boldsymbol{y}_3) - S_6(\boldsymbol{x}_1,\boldsymbol{x}_2,\boldsymbol{x}_3,\boldsymbol{x}_4\boldsymbol{y}_2,\boldsymbol{y}_1)S_2(\boldsymbol{y}_4,\boldsymbol{y}_3) - S_6(\boldsymbol{y}_4,\boldsymbol{y}_3,\boldsymbol{y}_2,\boldsymbol{y}_1,\boldsymbol{x}_2,\boldsymbol{x}_1)S_2(\boldsymbol{x}_4,\boldsymbol{x}_3)]. \quad (66)$$

We can see that the SPS cross section (62) is expressed in terms of dipoles, quadrupoles, sextupoles, and octupole scattering amplitudes.

2. Fragmentation of heavy quarks into heavy quarkonia

The fragmentation mechanism formally is also induced by a single-gluon scattering, with subsequent fragmentation of the produced heavy quarks into quarkonia states, as shown schematically in Fig. 5. A naive evaluation of the impact factor suggests that this mechanism should be dominant in the leading order in α_s, exceeding the contribution found in the previous section. However, as was discussed in Ref. [57], each fragmentation function of heavy quarks into the final-state quarkonium in the heavy quark mass limit is suppressed by factor $\sim\alpha_s^2(m_Q)$. For this reason, the cross section of this mechanism is suppressed as $\sim\alpha_s^5(m_Q)$, and is smaller by factor $\sim\alpha_s^2(m_Q)$ than the contribution discussed in Sec. II C 1. Nevertheless, for the sake of completeness, we will provide in this subsection the analytic results for the cross section of the process. Both for the single-hadron and dihadron fragmentation shown schematically in Fig. 5, the cross section can be represented as a convolution of the heavy quark pair production cross section, and the dihadron or a product of two single-hadron fragmentation functions, namely

$$\frac{d\sigma_T(p+p\to M_1+M_2+X)}{dy_1 d^2\boldsymbol{p}_1^\perp dy_2 d^2\boldsymbol{p}_2^\perp} = \int_0^1 \frac{dz_1}{z_1^2}\int_0^1 \frac{dz_2}{z_2^2}[D_f(z_1)D_f(z_2)+D_f(z_1,z_2)]\frac{d\sigma_T(p+p\to Q_1+Q_2+X)}{d\mathfrak{y}_1 d^2\boldsymbol{\ell}_{1,\perp} d\mathfrak{y}_2 \boldsymbol{\ell}_{2,\perp}}, \quad (67)$$

where $D_f(z)$ and $D_f(z_1,z_2)$ are the corresponding single- and dihadron fragmentation functions, and z_i are the fractions of the quark momentum carried by the quarkonium. At present, the dihadron fragmentation function $D_f(z_1,z_2)$ is not known. In the heavy quark mass limit, we may expect that for the charmonia-bottomonia pairs, the dihadron fragmentation function is very small,[1] so for the sake of simplicity, we will disregard its contribution and focus on the first term in the brackets of Eq. (67). The kinematic variables $(\mathfrak{y}_a,\boldsymbol{\ell}_a)$ in the right-hand side of Eq. (67) stand for the rapidities and transverse momenta of heavy quarks. In general, these variables do not coincide with quarkonium rapidities and transverse momenta $(y_a,\boldsymbol{p}_a)$, due to the fact that the observed heavy meson has only a fraction of the heavy quark momentum. For independent fragmentation from two heavy quarks, the relation of these two sets of variables is given by

$$\mathfrak{y}_i = y_i + \ln(1/z_i), \qquad \boldsymbol{\ell}_{i,\perp} = \boldsymbol{p}_i^\perp/z_i. \quad (68)$$

This relation implies that the integrals over z_1, z_2 in Eq. (67) should be regularized (cut) at the lower limit, which may be fixed from the condition that the sum of energies of two heavy quarks should not exceed the energy of the incoming gluon. However, in the high-energy kinematics, we expect that the energy of the incoming gluon is very large, so this correction can be disregarded.

The cross section of the $pp\to\bar{Q}QX$ subprocess has been found in the CGC framework [58] and is given by

$$\frac{d\sigma(p+p\to Q_1+Q_2+X)}{d\mathfrak{y}_1 d^2\boldsymbol{\ell}_{1,\perp} d\mathfrak{y}_2 \boldsymbol{\ell}_{2,\perp}} = \frac{x_1 g(x_1)}{(2\pi)^4}\int d^8\boldsymbol{X} e^{-i(\boldsymbol{\ell}_{1\perp}+\boldsymbol{\ell}_{2\perp})\cdot(\boldsymbol{b}_{12}-\boldsymbol{b}_{12'})} e^{-i(\bar{\alpha}\boldsymbol{\ell}_{1\perp}-\alpha\boldsymbol{\ell}_{2\perp})\cdot(\boldsymbol{r}_{12}-\boldsymbol{r}_{12'})} \times \alpha(1-\alpha)\sum_\lambda R_\lambda(\alpha,\boldsymbol{r}_{12},\boldsymbol{r}_{12'},Q^2)\Xi_{\mathrm{LO}}(\boldsymbol{x}_1,\boldsymbol{x}_2,\boldsymbol{x}_3,\boldsymbol{x}_4), \quad (69)$$

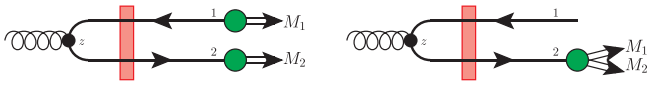


FIG. 5. Diagrams describing the heavy quarkonia pair production via single- and dihadron fragmentation in the leading order in α_s. The red block represents the interaction with the target (shock wave).

[1] If we assume that a perturbative treatment is applicable for evaluation of the dihadron fragmentation function, it is possible to show that in the heavy quark mass limit, the dihadron fragmentation function is suppressed by $\sim m_Q^{-4}$ compared to the product of two single-hadron fragmentation functions due to additional propagators.

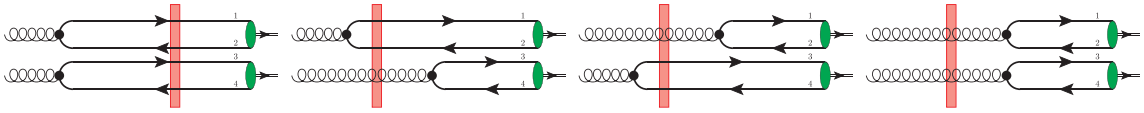


FIG. 6. Diagrams describing the inclusive charmonia-bottomonia pair production from a pair of the primordial gluons (double-parton scattering mechanism). Diagrams 2–4 include production of one of the heavy $\bar{Q}Q$ pairs in the color octet state and thus can be disregarded due to the smallness of color octet LDME. For the quarkonia pairs with the same hidden flavor, this mechanism should be supplemented with additional contributions in which the heavy quarks (1,3) are permuted. The red block represents the interaction with the target (shock wave).

where $d^8\boldsymbol{X}$ implies integration over the transverse coordinates of the heavy quarks in the amplitude and its conjugate (we use notations $\boldsymbol{x}_1, \boldsymbol{x}_2$ for the coordinates in the amplitude, and $\boldsymbol{x}'_1, \boldsymbol{x}'_2$ for its conjugate). We also defined the relative distances and pairwise impact parameters as

$$\boldsymbol{r}_{12} = \boldsymbol{x}_1 - \boldsymbol{x}_2, \qquad \boldsymbol{r}'_{12} = \boldsymbol{x}'_1 - \boldsymbol{x}'_2, \qquad \boldsymbol{b}_{12} = \alpha\boldsymbol{x}_1 + \bar{\alpha}\boldsymbol{x}_2, \qquad \boldsymbol{b}'_{12} = \alpha\boldsymbol{x}'_1 + \bar{\alpha}\boldsymbol{x}'_2, \tag{70}$$

where the variable α is the light-cone fraction of the gluon momentum carried by the quark,

$$\alpha = \frac{m_{1,\perp} e^{\mathfrak{y}_1}}{m_{1,\perp} e^{\mathfrak{y}_1} + m_{2,\perp} e^{\mathfrak{y}_2}}, \quad \text{where } m_{a,\perp} = \sqrt{m_b^2 + (\boldsymbol{\ell}_{a,\perp})^2}. \tag{71}$$

The impact factor R_λ can be evaluated using the CGC rules from Table I and the general procedure outlined at the end of Sec. II B. The final result of this procedure yields [59,60]

$$R_T(\alpha, \boldsymbol{r}_{12}, \boldsymbol{r}'_{12}, Q^2) = \frac{\alpha_s}{4\pi^2}\{\epsilon_f^2 K_1(\epsilon_f r_{12}) K_1(\epsilon_f r'_{12})[\alpha^2 + (1-\alpha)^2]\hat{\boldsymbol{r}}_{12}\cdot\hat{\boldsymbol{r}}'_{12} + m_f^2 K_0(\epsilon_f r_{12}) K_0(\epsilon_f r'_{12})\} \tag{72}$$

$$R_L(\alpha, \boldsymbol{r}_{12}, \boldsymbol{r}'_{12}, Q^2) = \frac{\alpha_s}{4\pi^2}\{4Q^2\alpha^2(1-\alpha)^2 K_0(\epsilon_f r_{12}) K_0(\epsilon_f r'_{12})\}. \tag{73}$$

The interaction with the target in the leading order does not depend on the helicity of the incoming gluon, and in the large-N_c limit reduces to

$$\begin{aligned}\Xi_{\mathrm{LO}} = \frac{1}{N_c^2 - 1}[&S_4(Y, \boldsymbol{x}_1, \boldsymbol{x}_2, \boldsymbol{x}_2{}', \boldsymbol{x}_1{}') + N_c^2 S_2(\boldsymbol{x}_2{}', \boldsymbol{x}_2) S_2(\boldsymbol{x}_1, \boldsymbol{x}_1{}') - N_c^2 S_2(\boldsymbol{x}_1, \boldsymbol{x}'_{12}) S_2(\boldsymbol{x}'_{12}, \boldsymbol{x}_2) \\ &- N_c^2 S_2(\boldsymbol{x}_1{}', \boldsymbol{x}_{12}) S_2(\boldsymbol{x}_{12}, \boldsymbol{x}'_2) + S_2(\boldsymbol{x}_1{}', \boldsymbol{x}'_2) + S_2(\boldsymbol{x}_1, \boldsymbol{x}_2) + N_c^2 S_2(\boldsymbol{x}_{12}, \boldsymbol{x}'_{12}) S_2(\boldsymbol{x}'_{12}, \boldsymbol{x}_{12}) - 1].\end{aligned} \tag{74}$$

According to our preliminary estimates, done with the fragmentation functions from Refs. [57,61–64], the contribution of this mechanism constitutes 5%–20% of the experimentally observed cross section in the kinematics of small transverse momenta p_T and in the p_T-integrated cross sections, in agreement with expected suppression by factor $\sim\alpha_s^2(m_Q)$. However, these estimates have significant dependence on the chosen parametrization of the fragmentation function, and also require modeling of the so far unknown dihadron (diquarkonium) fragmentation functions. In view of this, predictions for this mechanism will be presented elsewhere.

D. Charmonia-bottomonia production via double-parton scattering

The production of the charmonia-bottomonia pairs via the double-parton scattering proceeds via a mechanism that can be schematically represented by the diagrams shown in Fig. 6. As explained in the previous section, due to the smallness of the color octet LDMEs, it is possible to disregard completely the contributions of diagrams 2–4 and focus only on the first diagram.[2] The evaluation of the cross section largely repeats a similar evaluation of the inclusive single quarkonia production from Ref. [65]. The final result for the cross section may be represented as

[2]A full expression with account of color octet contributions may be found in Ref. [65].

$$\frac{d\sigma(p+p\to M_1+M_2+X)}{dy_1 d^2\boldsymbol{p}_1^\perp dy_2 d^2\boldsymbol{p}_2^\perp}=\frac{xg_f(x_1,\quad x_2)}{4}\int\prod_{k=1}^{4}d^2\boldsymbol{x}_k d^k\boldsymbol{y}_k e^{-i(\boldsymbol{p}_1-\boldsymbol{q}_{1,\perp})\cdot(\boldsymbol{x}_1+\boldsymbol{x}_2+\boldsymbol{y}_1+\boldsymbol{y}_2)}e^{-i(\boldsymbol{p}_2-\boldsymbol{q}_{2,\perp})\cdot(\boldsymbol{x}_3+\boldsymbol{x}_4+\boldsymbol{y}_3+\boldsymbol{y}_4)}$$
$$\times R_{M_1}(\boldsymbol{x}_1,\boldsymbol{x}_2,\boldsymbol{y}_1,\boldsymbol{y}_2)R_{M_2}(\boldsymbol{x}_3,\boldsymbol{x}_4,\boldsymbol{y}_3,\boldsymbol{y}_4)$$
$$\times[S_4(\boldsymbol{x}_1,\boldsymbol{x}_2,\boldsymbol{y}_1,\boldsymbol{y}_2)-S_2(\boldsymbol{x}_1,\boldsymbol{x}_2)S_2(\boldsymbol{y}_1,\boldsymbol{y}_2)][S_4(\boldsymbol{x}_3,\boldsymbol{x}_4,\boldsymbol{y}_3,\boldsymbol{y}_4)-S_2(\boldsymbol{x}_3,\boldsymbol{x}_4)S_2(\boldsymbol{y}_3,\boldsymbol{y}_4)],\quad(75)$$

where $g_f(x_1,x_2)$ is the so-called double-parton distribution function of the gluon, the impact factors R_{M_1} and R_{M_2} are the impact factors of the single-quarkonium production found in Ref. [65]. After adjustment of notations and omission of the relative motion of the quarks in the quarkonium, the impact factors for the S-wave quarkonia are given explicitly by

$$R_{M_a}(\boldsymbol{x}_1,\boldsymbol{x}_2,\boldsymbol{y}_1,\boldsymbol{y}_2)=\mathcal{M}^*_{M_a}(\boldsymbol{y}_1,\boldsymbol{y}_2)\mathcal{M}_{M_a}(\boldsymbol{x}_1,\boldsymbol{x}_2),\quad a=1,2\quad(76)$$

$$\mathcal{M}_{M_a}(\boldsymbol{x}_1,\boldsymbol{x}_2)=(ig)\int\frac{dk^-d^2\boldsymbol{k}}{(2\pi)^3}e^{i(\boldsymbol{k}-\frac{p_a^\perp-\boldsymbol{q}_{a,\perp}}{2})\cdot(\boldsymbol{x}_1-\boldsymbol{x}_2)}\mathrm{Tr}\left[\Pi_{M_a}^{S,S_z}\gamma^+S\left(\frac{p_a}{2}-k\right)\hat{\varepsilon}(\boldsymbol{q}_a)S\left(\frac{p_a}{2}-k-\boldsymbol{q}_a\right)\gamma^+\right]$$
$$=-(ig)\int\frac{d^2\boldsymbol{k}}{(2\pi)^2}e^{-i\boldsymbol{k}\cdot(\boldsymbol{x}_1-\boldsymbol{x}_2)/2}\frac{\mathrm{Tr}[\Pi_{M_a}^{S,S_z}\gamma^+(\frac{\hat{p}_a}{2}-\hat{k}+m_a)\hat{\varepsilon}(\boldsymbol{q}_a)(\frac{\hat{p}_a}{2}-\hat{k}-\hat{\boldsymbol{q}}_a+m_a)\gamma^+]}{p_a^+[(\frac{p_a^\perp}{2}-\boldsymbol{k})^2+m_a^2]+p_a^+[(\frac{p_a^\perp}{2}-\boldsymbol{k}-\boldsymbol{q}_{a,\perp})^2+m_a^2]},\quad(77)$$

where $\varepsilon(\boldsymbol{q}_a)$ is the polarization vector of the incoming gluon, the four-vector k^μ is defined as change of the quark momentum after interaction with the shock wave, and at the last step we applied the Cauchy theorem for the integration over k^-. We also took into account that in eikonal approximation $\boldsymbol{q}_a^+=p_a^+$, since the interaction with the shock wave does not change the plus component of the momentum. Using the procedure described at the end of Sec. II B and introducing the helicity projectors $\bar{\Pi}_{M_a}^{h_1,h_2}$ defined in Eq. (42), we may obtain

$$\mathcal{M}_{M_a}(\boldsymbol{x}_1,\boldsymbol{x}_2)=\bar{\Pi}_{M_1}^{h_1,h_2}\int\frac{d^2\boldsymbol{k}}{(2\pi)^2}\frac{(-ig)\mathrm{Tr}[\bar{u}_{h_1}(\frac{\hat{p}_a}{2}-\hat{k})\hat{\varepsilon}(\boldsymbol{q}_a)v_{h_2}(\frac{p_a}{2}-k-\boldsymbol{q}_a)]e^{i(\boldsymbol{k}-\frac{p_a^\perp-\boldsymbol{q}_{a,\perp}}{2})\cdot(\boldsymbol{x}_1-\boldsymbol{x}_2)}}{p_a^+[(\frac{p_a^\perp}{2}-\boldsymbol{k})^2+m_a^2]+p_a^+[(\frac{p_a^\perp}{2}-\boldsymbol{k}-\boldsymbol{q}_{a,\perp})^2+m_a^2]}.\quad(78)$$

The integral over $\boldsymbol{k}_\perp$ yields the well-known result for the wave function of $\bar{Q}Q$ in the photon evaluated in Refs. [59,60], namely

$$\int\frac{d^2\boldsymbol{k}}{(2\pi)^2}\frac{(-ig)\mathrm{Tr}[\bar{u}_{h_1}(\frac{p_a}{2}-k)\hat{\varepsilon}(\boldsymbol{q}_a)v_{h_2}(\boldsymbol{q}_a+k-\frac{p_a}{2})]e^{i(\boldsymbol{k}-\frac{p_a^\perp-\boldsymbol{q}_{a,\perp}}{2})\cdot(\boldsymbol{x}_1-\boldsymbol{x}_2)}}{p_a^+[(\frac{p_a^\perp}{2}-\boldsymbol{k})^2+m^2]+p_a^+[(\frac{p_a^\perp}{2}-\boldsymbol{k}-\boldsymbol{q}_{a,\perp})^2+m^2]}$$
$$=\sim\frac{-ig}{(2\pi)}[(\delta_{\lambda_a,h_1}-\delta_{\lambda_a,-h_1})\delta_{h_1,-h_2}i\boldsymbol{\varepsilon}_{\lambda_a}\cdot\nabla-m\sqrt{2}\mathrm{sign}(h_1)\delta_{\lambda_a,h_1}\delta_{h_1,h_2}]K_0(\bar{m}_a r_{12}),\qquad r_{12}=|\boldsymbol{x}_1-\boldsymbol{x}_2|,\quad(79)$$

where λ_a is the helicity of the incoming gluon and $\bar{m}_a=\sqrt{m_a^2+\boldsymbol{q}_a^2/4}$. The interaction of the partonic ensemble with the target (shock wave) is encoded in the correlator of Wilson lines which appears in the last line of Eq. (75). In the large-N_c limit and in heavy nuclei, it is possible to factorize it and rewrite as

$$\langle[S_4(\boldsymbol{x}_1,\boldsymbol{x}_2,\boldsymbol{y}_1,\boldsymbol{y}_2)-S_2(\boldsymbol{x}_1,\boldsymbol{x}_2)S_2(\boldsymbol{y}_1,\boldsymbol{y}_2)][S_4(\boldsymbol{x}_3,\boldsymbol{x}_4,\boldsymbol{y}_3,\boldsymbol{y}_4)-S_2(\boldsymbol{x}_3,\boldsymbol{x}_4)S_2(\boldsymbol{y}_3,\boldsymbol{y}_4)]\rangle$$
$$=\kappa\langle[S_4(\boldsymbol{x}_1,\boldsymbol{x}_2,\boldsymbol{y}_1,\boldsymbol{y}_2)-S_2(\boldsymbol{x}_1,\boldsymbol{x}_2)S_2(\boldsymbol{y}_1,\boldsymbol{y}_2)]\rangle\langle[S_4(\boldsymbol{x}_3,\boldsymbol{x}_4,\boldsymbol{y}_3,\boldsymbol{y}_4)-S_2(\boldsymbol{x}_3,\boldsymbol{x}_4)S_2(\boldsymbol{y}_3,\boldsymbol{y}_4)]\rangle,\quad(80)$$

where κ is some numerical parameter, and angular brackets imply averaging defined in Eq. (13). We may observe that the second line of Eq. (80) essentially factorizes onto a product of the structures $\langle S_4-S_2\otimes S_2\rangle$, which appear in the single-quarkonium production [65]. Furthermore, as was discussed in Ref. [66], at high energies it is possible to disregard small correlations of the gluons in the projectile and approximate the gluonic DPDF in the first line of Eq. (75) as

$$xg_f(x_1,x_2)\approx xg_f(x_1)xg_f(x_2).\quad(81)$$

In this approximation, we may recover the so-called pocket formula

$$\frac{d\sigma(p+p\to M_1+M_2+X)}{dy_1 d^2\boldsymbol{p}_1^\perp dy_2 d^2\boldsymbol{p}_2^\perp} \approx \kappa \frac{d\sigma(p+p\to M_1+X)}{dy_1 d^2\boldsymbol{p}_1^\perp}\frac{d\sigma(p+p\to M_2+X)}{dy_2 d^2\boldsymbol{p}_2^\perp}, \quad (82)$$

where the parameter κ is usually replaced with the so-called (inverse) effective cross section

$$\kappa = \sigma_{\rm eff}^{-1}, \quad (83)$$

which was introduced in the context of double-parton scattering in the k_T factorization framework (see the review in Ref. [22]). These findings demonstrate that description of the double-parton scattering in the CGC picture largely agrees with results of other frameworks.

III. NUMERICAL ESTIMATES FOR THE CROSS SECTION

A. Results for cross sections

For the sake of definiteness, we will focus on the production of the $1S$ quarkonia production, which are expected to have the largest cross section among all the charmonia-bottomonia pairs. We disregard the color octet channels in view of the smallness of color octet LDMEs (see, however, discussion in Refs. [4,53,67,68] about their significant uncertainty). For the dominant color singlet LDMEs, we will use the values [53,69,70]

$$\langle \mathcal{O}^{J/\psi}({}^3S_1^{[1]})\rangle \approx 1.16\ \text{GeV}^3,$$
$$\langle \mathcal{O}^{\Upsilon(1S)}({}^3S_1^{[1]})\rangle \approx 8.39\ \text{GeV}^3. \quad (84)$$

In agreement with NRQCD and potential models [71–74], these LDMEs approximately scale with heavy quark mass as $\sim(\alpha_s(m_Q)m_Q)^3$. As we demonstrated in the previous sections, the cross section of the charmonia-bottomonia production depends on a number of multipole correlators $S_{2n}(\boldsymbol{x}_1,\ldots,\boldsymbol{x}_{2n})$ defined in Eq. (16). For the dipole amplitude ($n=1$), we will use the phenomenological impact parameter b-dependent "bCGC" parametrization with the set parameters from Ref. [7] corresponding to a charm mass $m_c \approx 1.4$ GeV, as follows:

$$N(x,\boldsymbol{r},\boldsymbol{b}) = \begin{cases} N_0\left(\frac{rQ_s(x)}{2}\right)^{2\gamma_{\rm eff}(r)}, & r \le \frac{2}{Q_s(x)} \\ 1-\exp\left(-\mathcal{A}\ln\left(\mathcal{B}rQ_s\right)\right), & r > \frac{2}{Q_s(x)} \end{cases}, \quad (85)$$

$$\mathcal{A} = -\frac{N_0^2\gamma_s^2}{(1-N_0)^2\ln(1-N_0)}, \qquad \mathcal{B} = \frac{1}{2}(1-N_0)^{-\frac{1-N_0}{N_0\gamma_s}}, \quad (86)$$

$$Q_s(x,\boldsymbol{b}) = \left(\frac{x_0}{x}\right)^{\lambda/2} T_G(b), \qquad \gamma_{\rm eff}(r) = \gamma_s + \frac{1}{\kappa\lambda Y}\ln\left(\frac{2}{rQ_s(x)}\right), \qquad T_G(b) = \exp\left(-\frac{b^2}{4\gamma_s B_{\rm CGC}}\right) \quad (87)$$

$$\gamma_s = 0.6492, \qquad \lambda = 0.2023, \qquad x_0 = 6.9\times 10^{-4}, \qquad B_{\rm CGC} = 5.5\ \text{GeV}^{-2} \approx (0.463\ \text{fm})^2. \quad (88)$$

The higher-order amplitudes in general are independent nonperturbative objects, which can be related to a dipole amplitude under additional assumptions. In the McLerran-Venugopalan model, the weighting functional $W[\rho]$ has a Gaussian form, and for this reason all $2n$-leg correlators $S_{2n}(\boldsymbol{x}_1,\ldots,\boldsymbol{x}_{2n})$ reduce to pairwise products of dipole amplitudes S_2, summed over different permutations of $\boldsymbol{x}_1,\ldots.\boldsymbol{x}_{2n}$, namely

$$\langle U^\dagger(\boldsymbol{y}_1)^{a_1b_1}U(\boldsymbol{y}_2)^{a_2b_2}\ldots U^\dagger(\boldsymbol{y}_{2n-1})^{a_{2n-1}b_{2n-1}}U(\boldsymbol{y}_{2n})^{a_{2n}b_{2n}}\rangle \approx \sum_{\sigma\in\Pi(\chi)}\prod_{\{\alpha,\beta\}\in\sigma}\langle U^\dagger(\boldsymbol{y}_\alpha)^{a_\alpha b_\alpha}U(\boldsymbol{y}_\beta)^{a_\beta b_\beta}\rangle, \quad (89)$$

where $\chi=\{1,2,\ldots,2n\}$ and $\Pi(\chi)$ is the set of partitions of χ with disjoint pairs. The result (89) essentially allows us to use Wick's theorem for evaluation of the diagrams with multipole contributions. The expression (89) sometimes is also justified using Kovner's *area enhancement argument* introduced in Refs. [75–77]: the color group averaging suppresses all configurations except those in which a small group of partons have a net zero color charge and are tightly clustered, with relative distances constrained by $|\boldsymbol{x}_i-\boldsymbol{x}_j| \lesssim Q_s^{-1}$, where Q_s is the saturation scale; in the phase space integral, the largest phase spaces have color singlet quark-antiquark pairs. The advantage of the area law argument is that it does not rely on specific choice of the weighting functional $W[\rho]$. However, the ansatz (89) may

be not compatible with the JIMWLK evolution equation: as was found in Refs. [78–80] solving the JIMWLK equations for the quadrupoles in the limit of large number of colors $N_c \gg 1$, the corresponding solution can be described in terms of dipole amplitudes, though the general expression is much more complicated and does not reduce to Eq. (89). Similar solutions of the JIMWLK equations in the large-N_c limit are also known for the sextupoles and octupoles [81,82], and in general they also do not coincide with Eq. (89). The large-N_c solution of the JIMWLK equation coincides with Eq. (89) for the configuration of small well-separated pairs of quark-antiquarks, as expected from area enhancement argument. However, for charmonia-bottomonia production, we found that this argument does not work because the impact factors of SPS production select configurations with approximately the same distances between heavy partons. At the same time, using the large-N_c solutions directly is prohibitively expensive: as could be seen from Eq. (62), the evaluation of the cross section requires taking the integral in 16 dimensions, and the explicit expressions for higher-order multipoles from Refs. [81,82] include hundreds of terms with nontrivial behavior along various hypersurfaces in 16-dimensional space.

Fortunately, it is possible to simplify analysis in the so-called dilute (weak scattering) limit [78,79], which may be applicable at moderately high energies, as well as in the heavy quark mass limit, when the mass m_Q exceeds significantly the saturation scale Q_s, and thus the distance between heavy quarks is given by $|\boldsymbol{x}_i - \boldsymbol{x}_j| \sim m_Q^{-1} \ll Q_s^{-1}$. In this regime, we may approximate the Wilson lines (11) as

$$U(\boldsymbol{x}) \approx 1 + ig \int dx^- A_a^+(x^-, \boldsymbol{x}_\perp) t^a + \frac{(ig)^2}{2} P \int dx_1^- A_a^+(x_1^-, \boldsymbol{x}_\perp) t^a \int dx_1^- A_b^+(x_2^-, \boldsymbol{x}_\perp) t^b, \tag{90}$$

and obtain for the dipole S-matrix element

$$S_2(Y, \boldsymbol{x}_1, \boldsymbol{x}_2) \equiv \frac{1}{N_c} \langle \mathrm{tr}(U(\boldsymbol{x}_1) U^\dagger(\boldsymbol{x}_2)) \rangle_Y \approx 1 - \frac{\langle |\alpha_a(\boldsymbol{x}_1) - \alpha_a(\boldsymbol{x}_2)|^2 \rangle}{4N_c}, \qquad \alpha_a(\boldsymbol{x}) = g \int dx^- A_a^+(x^-, \boldsymbol{x}_\perp) t^a, \tag{91}$$

so the forward dipole scattering amplitude can be approximated as

$$N(\boldsymbol{r}_{12}, \boldsymbol{b}_{12}) \equiv 1 - S_2(\boldsymbol{x}_1, \boldsymbol{x}_2) = \frac{\langle |\alpha_a(\boldsymbol{x}_1) - \alpha_a(\boldsymbol{x}_2)|^2 \rangle}{4N_c}, \tag{92}$$

where we defined the relative distance and the average center of mass position using $\boldsymbol{r}_{ij} = \boldsymbol{x}_i - \boldsymbol{x}_j$, $\boldsymbol{b}_{ij} = (\alpha_i \boldsymbol{x}_i + \alpha_j \boldsymbol{x}_j)/(\alpha_i + \alpha_j)$. The expression for the quadrupole matrix element S_4 in this limit is given by [78,79]

$$\begin{aligned} S_4 \equiv \left\langle \frac{1}{N_c} \mathrm{tr}_c [U(\boldsymbol{x}_1) U^\dagger(\boldsymbol{x}_2) U(\boldsymbol{x}_3) U^\dagger(\boldsymbol{x}_4)] \right\rangle &\approx 1 - N(x, \boldsymbol{r}_{12}, \boldsymbol{b}_{12}) - N(x, \boldsymbol{r}_{34}, \boldsymbol{b}_{34}) \\ &- N(x, \boldsymbol{r}_{23}, \boldsymbol{b}_{23}) - N(x, \boldsymbol{r}_{14}, \boldsymbol{b}_{14}) + N(x, \boldsymbol{r}_{13}, \boldsymbol{b}_{13}) + N(x, \boldsymbol{r}_{24}, \boldsymbol{b}_{24}). \end{aligned} \tag{93}$$

The expressions for $T_a^{(4)}, T_a^{(4')}, T_a^{(8)}$ defined in Eqs. (32)–(34) simplify in this limit as

$$T_a^{(4)}(\boldsymbol{x}_1, \boldsymbol{x}_2, \boldsymbol{x}_3, \boldsymbol{x}_4) \approx T_a^{(4')}(\boldsymbol{x}_1, \boldsymbol{x}_2, \boldsymbol{x}_3, \boldsymbol{x}_4) \approx \frac{i}{4} [\alpha_a(\boldsymbol{x}_3) - \alpha_a(\boldsymbol{x}_4)], \tag{94}$$

whereas the convolutions of two $T_a^{(4)}$ with different arguments can be expressed in terms of the dipole forward scattering amplitude as

$$\frac{8}{N_c} T_a^{(4)}(\boldsymbol{x}_1, \boldsymbol{x}_2, \boldsymbol{x}_3, \boldsymbol{x}_4) T_a^{(4)}(\boldsymbol{x}_{1'}, \boldsymbol{x}_{2'}, \boldsymbol{x}_{3'}, \boldsymbol{x}_{4'}) = N(\boldsymbol{r}_{3,3'}, \boldsymbol{b}_{3,3'}) + N(\boldsymbol{r}_{4,4'}, \boldsymbol{b}_{4,4'}) - N(\boldsymbol{r}_{3,4'}, \boldsymbol{b}_{3,4'}) - N(\boldsymbol{r}_{4,3'}, \boldsymbol{b}_{4,3'}). \tag{95}$$

The combination of dipoles and quadrupoles which appear in DPS cross section (75) can be simplified as

$$S_4(\boldsymbol{x}_1, \boldsymbol{x}_2, \boldsymbol{x}_3, \boldsymbol{x}_4) - S_2(\boldsymbol{x}_1, \boldsymbol{x}_2) S_2(\boldsymbol{x}_3, \boldsymbol{x}_4) \approx N(x, \boldsymbol{r}_{13}, \boldsymbol{b}_{13}) + N(x, \boldsymbol{r}_{24}, \boldsymbol{b}_{24}) - N(x, \boldsymbol{r}_{23}, \boldsymbol{b}_{23}) - N(x, \boldsymbol{r}_{14}, \boldsymbol{b}_{14}). \tag{96}$$

The suppression of the dipole amplitude $N(x, \boldsymbol{r}, \boldsymbol{b})$ at large impact parameters is controlled by the behavior of the factor $T_G(b)$ defined in Eq. (87), and the effective cross section σ_{eff}, which corresponds to transverse area of the proton, can be estimated from

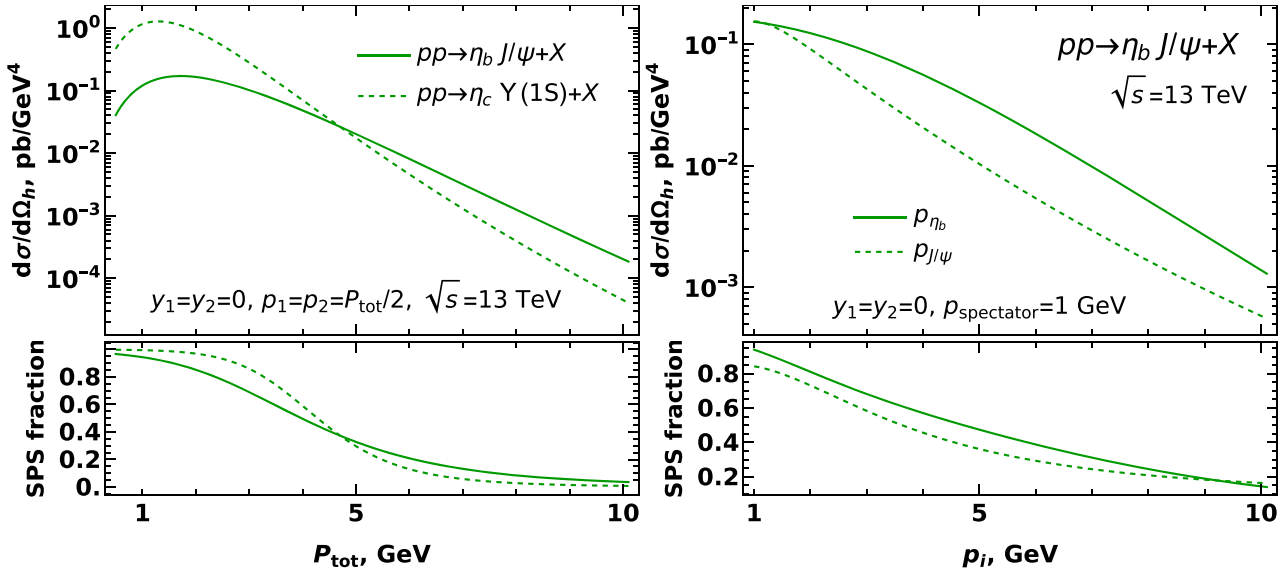


FIG. 7. Left: dependence of the cross section $d\sigma/d\Omega_h = d^4\sigma/dy_1 dp_1^2 dy_2 dp_2^2$ on the transverse momentum $P_{\rm tot}$ of the charmonium-bottomonium pair, assuming that it is shared equally between the final-state quarkonia. Right: dependence of the cross section on the transverse momentum of one of the quarkonia, assuming that the other has fixed transverse momentum $p = 1$ GeV. In the bottom panels of both plots, we show the relative contribution of the SPS mechanism, namely the ratio $d\sigma_{\rm SPS}/(d\sigma_{\rm SPS} + d\sigma_{\rm DPS})$. The tabulated data corresponding to this figure are available from the Supplementary Material [83].

$$\sigma_{\rm eff} \approx \pi\langle b^2\rangle = \pi \frac{\int d^2b b^2 T_G(b)}{\int d^2b T_G(b)} \approx 17.7 \text{ mb}, \quad (97)$$

in agreement with other phenomenological estimates. In this way, the cross section is fully determined by the dipole scattering amplitude $N(\boldsymbol{r}, \boldsymbol{b})$. In Fig. 7, we have shown the cross section as a function of the transverse momentum of the produced quarkonia at central rapidities. We found that the cross section decreases rapidly as a function of p_T of each quarkonium. As we can see in the bottom panels of this figure, the SPS mechanism dominates in the small-p_T domain; however, its relative contribution decreases at larger transverse momenta, in agreement with what was found in other approaches (see Ref. [22] for a review). In Fig. 8, we compare the cross section with recent experimental data from the LHCb [18]. We found that overall, the dilute approximation provides a reasonable description of the *shape* of the p_T-dependence. However, the normalization of the cross section, namely the value of

$$\sigma_{\rm tot} = \int dp_T \frac{d\sigma}{dp_T} \quad (98)$$

in dilute approximation is $\sigma_{\rm CGC}^{\rm (dilute)} \approx 86$ pb, which is ∼50% smaller than the experimentally measured value $\sigma_{\rm exp}^{\rm (LHCb)} = 133 \pm 22 \pm 7 \pm 3$ pb. These findings indicate that the suggested approach gives a fair qualitative description of the data, though still there is a space for improvement of the phenomenological parametrizations of the multipole matrix elements.

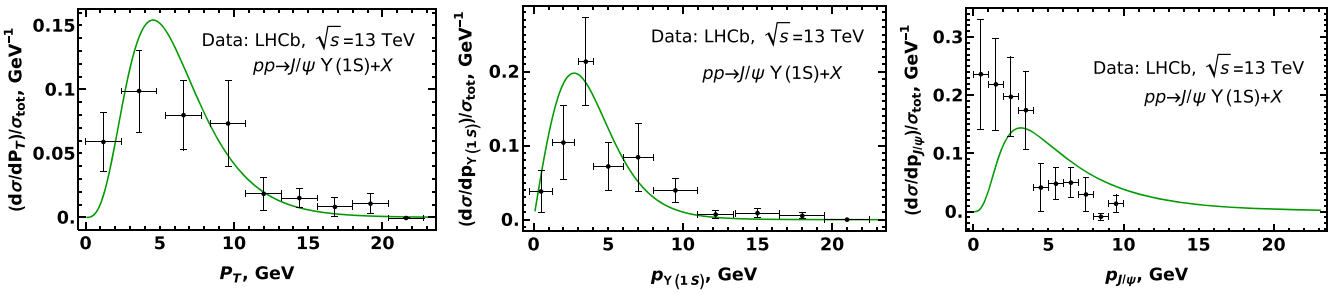


FIG. 8. Comparison of the CGC predictions (in dilute approximation) with experimental data from the LHCb [18]. Left: data for the cross-section as a function of the total momentum of charmonia-bottomonia pair. Center and right: dependence on the transverse momentum of one of the quarkonia, assuming that we integrated out the transverse momentum of another. Note that in all plots, we have shown the cross section normalized to $\sigma_{\rm tot}$, and the value of the latter is different for the theoretical and experimental results (see the text for more details). The tabulated data corresponding to this figure are available from the Supplementary Material [83].

IV. CONCLUSIONS

In this study, we applied the color glass condensate framework for analysis of the inclusive hadroproduction of heavy charmonia-bottomonia pairs in the LHC kinematics. We found that there are several complementary mechanisms which may be classified by number of gluons emitted from projectiles as single- and double-parton scattering. We evaluated explicitly the impact factors for the mechanisms which contribute in the leading order in α_s. For the DPS mechanism, the impact factors in the large-N_c limit factorize into a product of impact factors of single quarkonia, so the DPS contribution can be reduced to the well-known pocket formula. The contribution of SPS is more sophisticated and includes convolutions of impact factors with dipole, quadrupole, sextupole, and octupole scattering amplitudes (correlators of Wilson lines). While there are some formal solution parametrizations of these objects based on solutions of the JIMWLK equation, we could not use them for phenomenological estimates of the cross section due to their complexity and the excessive requirement of computational resources. However, preliminary phenomenological estimates of the cross sections in the simplified dilute approximation suggest that our approach provides a fair qualitative description of the LHCb data for $J/\psi + \Upsilon(1S)$ production.

ACKNOWLEDGMENTS

We thank our colleagues at UTFSM and Professor Ian Balitsky for encouraging and clarifying discussions. This research was partially supported by Proyecto ANID PIA/APOYO AFB220004 (Chile) and Fondecyt (Chile) Grants Regular No. 1220242 and No. 1251975. Powered@NLHPC: This research was partially supported by the supercomputing infrastructure of the NLHPC (ECM-02).

DATA AVAILABILITY

The data supporting this study's findings are available within the article.

[1] G. T. Bodwin, E. Braaten, and G. P. Lepage, Rigorous QCD analysis of inclusive annihilation and production of heavy quarkonium, Phys. Rev. D **51**, 1125 (1995); **55**, 5853(E) (1997).
[2] F. Maltoni, M. L. Mangano, and A. Petrelli, Quarkonium photoproduction at next-to-leading order, Nucl. Phys. **B519**, 361 (1998).
[3] N. Brambilla, E. Mereghetti, and A. Vairo, Hadronic quarkonium decays at order v^7, Phys. Rev. D **79**, 074002 (2009); **83**, 079904(E) (2011).
[4] Y. Feng, J. P. Lansberg, and J. X. Wang, Energy dependence of direct-quarkonium production in pp collisions from fixed-target to LHC energies: complete one-loop analysis, Eur. Phys. J. C **75**, 313 (2015).
[5] N. Brambilla *et al.*, Heavy quarkonium: Progress, puzzles, and opportunities, Eur. Phys. J. C **71**, 1534 (2011).
[6] H. Kowalski, L. Motyka, and G. Watt, Exclusive diffractive processes at HERA within the dipole picture, Phys. Rev. D **74**, 074016 (2006).
[7] A. H. Rezaeian and I. Schmidt, Impact-parameter dependent color glass condensate dipole model and new combined HERA data, Phys. Rev. D **88**, 074016 (2013).
[8] A. H. Rezaeian, M. Siddikov, M. Van de Klundert, and R. Venugopalan, Analysis of combined HERA data in the impact-parameter dependent saturation model, Phys. Rev. D **87**, 034002 (2013).
[9] S. J. Brodsky, G. Kopp, and P. M. Zerwas, Hadron production near threshold in photon-photon collisions, Phys. Rev. Lett. **58**, 443 (1987).
[10] G. P. Lepage and S. J. Brodsky, Exclusive processes in perturbative quantum chromodynamics, Phys. Rev. D **22**, 2157 (1980).
[11] C. Berger and W. Wagner, Photon-photon reactions, Phys. Rep. **146**, 1 (1987).
[12] M. S. Baek, S. Y. Choi, and H. S. Song, Exclusive heavy meson pair production at large recoil, Phys. Rev. D **50**, 4363 (1994).
[13] J. Badier *et al.* (NA3 Collaboration), Evidence for production in interactions at 150-GeV/c and 280-GeV/c, Phys. Lett. **114B**, 457 (1982).
[14] J. Badier *et al.* (NA3 Collaboration), $\psi\psi$ production and limits on beauty meson production from 400-GeV/c Protons, Phys. Lett. **158B**, 85 (1985).
[15] P. Ko, C. Yu, and J. Lee, Inclusive double-quarkonium production at the Large Hadron Collider, J. High Energy Phys. 01 (2011) 070.
[16] A. K. Likhoded, A. V. Luchinsky, and S. V. Poslavsky, Simultaneous production of charmonium and bottomonium mesons at the LHC, Phys. Rev. D **91**, 114016 (2015).
[17] H. S. Shao and Y. J. Zhang, Complete study of hadroproduction of a Υ meson associated with a prompt J/ψ, Phys. Rev. Lett. **117**, 062001 (2016).
[18] R. Aaij *et al.* (LHCb Collaboration), Associated production of prompt J/ψ and Υ mesons in pp collisions at $\sqrt{s} = 13$ TeV, J. High Energy Phys. 08 (2023) 093.
[19] V. M. Abazov *et al.* (D0 Collaboration), Evidence for simultaneous production of J/ψ and Υ mesons, Phys. Rev. Lett. **116**, 082002 (2016).
[20] I. Belyaev and D. Savrina, Study of double parton scattering processes with heavy quarks, in *Multiple Parton Interactions at the LHC*, Advanced Series on Directions in High Energy Physics (World Scientific, Singapore, 2018), pp. 141–157, 10.1142/9789813227767_0008.

[21] J. P. Lansberg and H. S. Shao, Associated production of a quarkonium and a Z boson at one loop in a quark-hadron-duality approach, J. High Energy Phys. 10 (2016) 153.
[22] J. P. Lansberg, New observables in inclusive production of quarkonia, Phys. Rep. **889**, 1 (2020).
[23] L. D. McLerran and R. Venugopalan, Computing quark and gluon distribution functions for very large nuclei, Phys. Rev. D **49**, 2233 (1994).
[24] L. D. McLerran and R. Venugopalan, Gluon distribution functions for very large nuclei at small transverse momentum, Phys. Rev. D **49**, 3352 (1994).
[25] L. D. McLerran and R. Venugopalan, Green's function in the color field of a large nucleus, Phys. Rev. D **50**, 2225 (1994).
[26] F. Gelis, E. Iancu, J. Jalilian-Marian, and R. Venugopalan, The color glass condensate, Annu. Rev. Nucl. Part. Sci. **60**, 463 (2010).
[27] E. Iancu and A. H. Mueller, From color glass to color dipoles in high-energy onium onium scattering, Nucl. Phys. **A730**, 460 (2004).
[28] C. A. Aidala *et al.*, Probing nucleons and nuclei in high energy collisions, arXiv:2002.12333.
[29] Y. Q. Ma and R. Venugopalan, Comprehensive description of J/ψ production in proton-proton collisions at collider energies, Phys. Rev. Lett. **113**, 192301 (2014).
[30] V. Cheung, Z. B. Kang, F. Salazar, and R. Vogt, Direct quarkonium production in DIS from a joint CGC and NRQCD framework, Phys. Rev. D **110**, 094039 (2024).
[31] H. Mäntysaari, K. Roy, F. Salazar, and B. Schenke, Gluon imaging using azimuthal correlations in diffractive scattering at the Electron-Ion Collider, Phys. Rev. D **103**, 094026 (2021).
[32] Z. B. Kang, E. Li, and F. Salazar, Direct quarkonium-plus-gluon production in DIS in the color glass condensate, arXiv:2310.12102.
[33] K. Tuchin, Heavy quark production by a quasiclassical color field in proton nucleus collisions, Phys. Lett. B **593**, 66 (2004).
[34] J. P. Blaizot, F. Gelis, and R. Venugopalan, High-energy pA collisions in the color glass condensate approach. 2. Quark production, Nucl. Phys. **A743**, 57 (2004).
[35] B. Abelev *et al.* (ALICE Collaboration), Transverse momentum distribution and nuclear modification factor of charged particles in p-Pb collisions at $\sqrt{s_{NN}} = 5.02$ TeV, Phys. Rev. Lett. **110**, 082302 (2013).
[36] G. Aad *et al.* (ATLAS Collaboration), Transverse momentum, rapidity, and centrality dependence of inclusive charged-particle production in $\sqrt{s_{NN}} = 5.02$ TeV $\mathrm{p}+\mathrm{Pb}$ collisions measured by the ATLAS experiment, Phys. Lett. B **763**, 313 (2016).
[37] G. Watt and H. Kowalski, Impact parameter dependent color glass condensate dipole model, Phys. Rev. D **78**, 014016 (2008).
[38] G. G. Da Silveira (ATLAS, LHCb, and CMS Collaborations), QCD probes at LHC, arXiv:1805.00772.
[39] J. L. Albacete, Testing the CGC in proton-lead collisions at the LHC, Nucl. Phys. **A910-911**, 155 (2013).
[40] R. Aaij *et al.* (LHCb Collaborations), Study of exclusive photoproduction of charmonium in ultra-peripheral lead-lead collisions, J. High Energy Phys. 06 (2023) 146.
[41] H. Mäntysaari, F. Salazar, and B. Schenke, Energy dependent nuclear suppression from gluon saturation in exclusive vector meson production, Phys. Rev. D **109**, L071504 (2024).
[42] L. V. Gribov, E. M. Levin, and M. G. Ryskin, Semihard processes in QCD, Phys. Rep. **100**, 1 (1983).
[43] A. H. Mueller and J. Qiu, Gluon recombination and shadowing at small values of x, Nucl. Phys. **B268**, 427 (1986).
[44] L. McLerran and R. Venugopalan, Gluon distribution functions for very large nuclei at small transverse momentum, Phys. Rev. D **49**, 3352 (1994); Green's function in the color field of a large nucleus, Phys. Rev. D **50**, 2225 (1994); Fock space distributions, structure functions, higher twists, and small x, Phys. Rev. D **59**, 09400 (1999).
[45] K. J. Golec-Biernat and M. Wusthoff, Saturation in diffractive deep inelastic scattering, Phys. Rev. D **60**, 114023 (1999).
[46] B. Z. Kopeliovich and A. V. Tarasov, Gluon shadowing in heavy flavor production off nuclei, Nucl. Phys. **A710**, 180 (2002).
[47] B. Kopeliovich, A. Tarasov, and J. Hufner, Coherence phenomena in charmonium production off nuclei at the energies of RHIC and LHC, Nucl. Phys. **A696**, 669 (2001).
[48] S. J. Brodsky, H. C. Pauli, and S. S. Pinsky, Quantum chromodynamics and other field theories on the light cone, Phys. Rep. **301**, 299 (1998).
[49] A. Ayala, M. Hentschinski, J. Jalilian-Marian, and M. E. Tejeda-Yeomans, Spinor helicity methods in high-energy factorization: efficient momentum-space calculations in the Color Glass Condensate formalism, Nucl. Phys. **B920**, 232 (2017).
[50] P. Caucal, F. Salazar, and R. Venugopalan, Dijet impact factor in DIS at next-to-leading order in the Color Glass Condensate, J. High Energy Phys. 11 (2021) 222.
[51] P. Caucal, F. Salazar, B. Schenke, and R. Venugopalan, Back-to-back inclusive dijets in DIS at small x: Sudakov suppression and gluon saturation at NLO, J. High Energy Phys. 11 (2022) 169.
[52] Y. V. Kovchegov and E. Levin, Quantum chromodynamics at high energy, Cambridge Monogr. Part. Phys., Nucl. Phys., Cosmol. **33**, 1 (2012).
[53] S. P. Baranov and A. V. Lipatov, Prompt charmonia production and polarization at the LHC in the NRQCD with k_T-factorization. III. J/ψ meson, Phys. Rev. D **96**, 034019 (2017).
[54] S. P. Baranov and A. V. Lipatov, Are there any challenges in the charmonia production and polarization at the LHC?, Phys. Rev. D **100**, 114021 (2019).
[55] S. Andrade, M. Siddikov, and I. Schmidt, Exclusive photoproduction of heavy quarkonia pairs, Phys. Rev. D **105**, 076022 (2022).
[56] T. Lappi and R. Paatelainen, The one loop gluon emission light cone wave function, Ann. Phys. (Amsterdam) **379**, 34 (2017).
[57] Y. Q. Ma, J. W. Qiu, and H. Zhang, Heavy quarkonium fragmentation functions from a heavy quark pair. I. S wave, Phys. Rev. D **89**, 094029 (2014).
[58] H. Fujii, C. Marquet, and K. Watanabe, Comparison of improved TMD and CGC frameworks in forward quark dijet production, J. High Energy Phys. 12 (2020) 181.

[59] H. G. Dosch, T. Gousset, G. Kulzinger, and H. J. Pirner, Vector meson leptoproduction and nonperturbative gluon fluctuations in QCD, Phys. Rev. D **55**, 2602 (1997).
[60] J. D. Bjorken, J. B. Kogut, and D. E. Soper, Quantum electrodynamics at infinite momentum: Scattering from an external field, Phys. Rev. D **3**, 1382 (1971).
[61] B. A. Kniehl and G.Kramer, Inclusive and production from decay in collisions, Phys. Rev. D **60**, 014006 (1999).
[62] Y. Q. Ma, J. W. Qiu, and H. Zhang, Heavy quarkonium fragmentation functions from a heavy quark pair. II. P-wave, Phys. Rev. D **89**, 094030 (2014).
[63] Q. L. Jia, A. P. Chen, and Y. G. Xu, Single parton fragmentation functions of heavy quarkonium in soft gluon factorization, Phys. Rev. D **109**, 034039 (2024).
[64] X. C. Zheng, X. G. Wu, and X. D. Huang, NLO fragmentation functions for a quark into a spin-singlet quarkonium: Same flavor case, J. High Energy Phys. 07 (2021) 014.
[65] Z. B. Kang, Y. Q. Ma, and R. Venugopalan, Quarkonium production in high energy proton-nucleus collisions: CGC meets NRQCD, J. High Energy Phys. 01 (2014) 056.
[66] K. Golec-Biernat, E. Lewandowska, M. Serino, Z. Snyder, and A. M. Stasto, Constraining the double gluon distribution by the single gluon distribution, Phys. Lett. B **750**, 559 (2015).
[67] M. Butenschoen, Z. G. He, and B. A. Kniehl, η_c production at the LHC challenges nonrelativistic-QCD factorization, Phys. Rev. Lett. **114**, 092004 (2015).
[68] S. P. Baranov, A. V. Lipatov, and N. P. Zotov, Prompt charmonia production and polarization at LHC in the NRQCD with k_T-factorization. Part I: $\psi(2S)$ meson, Eur. Phys. J. C **75**, 455 (2015).
[69] Y. Feng, B. Gong, L. P. Wan, and J. X. Wang, An updated study of Υ production and polarization at the Tevatron and LHC, Chin. Phys. C **39**, 123102 (2015).
[70] N. A. Abdulov and A. V. Lipatov, Bottomonium production and polarization in the NRQCD with k_T-factorization. III: $\Upsilon(1S)$ and $\chi_b(1P)$ mesons, Eur. Phys. J. C **81**, 1085 (2021).
[71] E. Eichten, K. Gottfried, T. Kinoshita, K. D. Lane, and T. M. Yan, Charmonium: The model, Phys. Rev. D **17**, 3090 (1978); **21**, 313(E) (1980).
[72] E. Eichten, K. Gottfried, T. Kinoshita, K. D. Lane, and T. M. Yan, Charmonium: Comparison with experiment, Phys. Rev. D **21**, 203 (1980).
[73] C. Quigg and J. L. Rosner, Quarkonium level spacings, Phys. Lett. **71B**, 153 (1977).
[74] A. Martin, A fit of upsilon and charmonium spectra, Phys. Lett. **93B**, 338 (1980).
[75] P. Agostini, T. Altinoluk, and N. Armesto, Multi-particle production in proton-nucleus collisions in the color glass condensate, Eur. Phys. J. C **81**, 760 (2021).
[76] A. Kovner and A. H. Rezaeian, Double parton scattering in the CGC: Double quark production and effects of quantum statistics, Phys. Rev. D **96**, 074018 (2017).
[77] A. Kovner and A. H. Rezaeian, Multiquark production in $p + A$ collisions: Quantum interference effects, Phys. Rev. D **97**, 074008 (2018).
[78] E. Iancu and D. N. Triantafyllopoulos, JIMWLK evolution in the Gaussian approximation, J. High Energy Phys. 04 (2012) 025.
[79] E. Iancu and D. N. Triantafyllopoulos, Higher-point correlations from the JIMWLK evolution, J. High Energy Phys. 11 (2011) 105.
[80] E. Iancu, QCD in heavy ion collisions, arXiv:1205.0579.
[81] F. Dominguez, C. Marquet, A. M. Stasto, and B. W. Xiao, Universality of multiparticle production in QCD at high energies, Phys. Rev. D **87**, 034007 (2013).
[82] Y. Shi, C. Zhang, and E. Wang, Multipole scattering amplitudes in the Color Glass Condensate formalism, Phys. Rev. D **95**, 116014 (2017).
[83] See Supplemental Material at http://link.aps.org/supplemental/10.1103/cz6q-3w6d for tabulated data which correspond to the results shown in the Figs. 7 and 8.